THE UNIVERSITY of EDINBURGH

Edinburgh Research Explorer

In-plane Elastic Flexibility of CLT Floor Diaphragms

Citation for published version:
D'Arenzo, G, Casagrande, D, Reynolds, T & Fossetti, M 2019, 'In-plane Elastic Flexibility of CLT Floor Diaphragms', *Construction and Building Materials*, vol. 209, pp. 709-724.
https://doi.org/10.1016/j.conbuildmat.2019.03.060

Digital Object Identifier (DOI):
10.1016/j.conbuildmat.2019.03.060

Link:
Link to publication record in Edinburgh Research Explorer

Document Version:
Peer reviewed version

Published In:
Construction and Building Materials

General rights
Copyright for the publications made accessible via the Edinburgh Research Explorer is retained by the author(s) and / or other copyright owners and it is a condition of accessing these publications that users recognise and abide by the legal requirements associated with these rights.

Take down policy
The University of Edinburgh has made every reasonable effort to ensure that Edinburgh Research Explorer content complies with UK legislation. If you believe that the public display of this file breaches copyright please contact openaccess@ed.ac.uk providing details, and we will remove access to the work immediately and investigate your claim.

Download date: 05. May. 2023

In-plane Elastic Flexibility of Cross Laminated Timber Floor Diaphragms

This is the author's postprint. The published article is: D'Arenzo, G. et al. (2019) 'In-plane elastic flexibility of cross laminated timber floor diaphragms', Construction and Building Materials. Elsevier Ltd, 209, pp. 709–724. dx.doi.org/10.1016/j.conbuildmat.2019.03.060.

Giuseppe D'Arenzo*[a], Daniele Casagrande[b], Thomas Reynolds[c], Marinella Fossetti[d]

[a]*Università Degli Studi Di Enna "Kore", Facoltà di Ingegneria ed Architettura, Italy; * Corresponding author, giuseppe.darenzo@unikore.it,*
[b]*Trees and Timber Institute - National Research Council of Italy (CNR-IVALSA), Italy; casagrande@ivalsa.cnr.it*
[c]*The University of Edinburgh, School of Engineering, Scotland, UK; t.reynolds@ed.ac.uk*
[d]*Università Degli Studi Di Enna "Kore", Facoltà di Ingegneria ed Architettura, Italy; marinella.fossetti@unikore.it*

Abstract

No appropriate method exists to calculate the in-plane flexibility of cross-laminated timber as a floor diaphragm. This flexibility affects the load distribution between shear walls, bracing or cores, as well as adding to local deflections and inter-storey drift. This paper presents a sensitivity analysis based on experimentally measured connection behaviour from the literature and the present study. An important new contributing factor is described: the connection of the floor panels to the supporting wall panels below allows the walls to act as top and bottom chords in the bending and shear of the panel. A new equivalent frame model is described to capture the significant mechanisms of deformation of the diaphragm, validated against a planar finite element model of the elastic behaviour of the panels and the connections between them. The low computational cost of the simplified model allows a wide sensitivity analysis to be carried out, and also makes it suitable for practical design calculations. The flexibility of the floors studied here was seen to be dominated by the slip between panels, rather than panel rotation or bending of the panels themselves. The supporting walls have a strong influence on the moment distribution, but do not strongly influence the slip between panels.

Keywords

Timber; CLT; Stiffness; Screwed Connections; Lateral Loads; Multi-Storey.

Highlights

- A new factor contributing the in-plane flexibility of CLT diaphragms is described;
- A thorough sensitivity analysis based on experimental results is presented;
- An equivalent frame model for CLT diaphragms is numerically validated.

1. Introduction and Background

Floor diaphragms play an important role in the lateral load resisting systems of buildings, distributing the applied force to the core, shear walls or bracing elements. If there are multiple elements resisting lateral load, then the distribution between those elements depends both on the relative stiffness of those elements, and on the stiffness of the diaphragm itself. In some cases, if the floor is relatively stiff, or has a short span between lateral load resisting elements, it is reasonable to assume rigid diaphragm action, and the force can be distributed to each element according to its stiffness [1]. Otherwise, an analysis is required which takes into account the stiffness of the floor.

If the floor is made from Cross Laminated Timber (CLT), then the stiffness of the diaphragm depends on several parameters: the orthotropic elastic properties of the panel, the load-slip behaviour of the connection between adjacent floor panels (floor-to-floor connections) and the load-slip behaviour of the connections to the vertical structure (floor-to-wall connections). From here on, the lateral load resisting system will be referred to as the shear wall (which may be part of a core), since that is the more common system in multi-storey Cross Laminated Timber construction.

The design of floor-to-floor and floor-to-wall connec-

tions are commonly performed by adopting a simplified approach considering the floors as a deep beam spanning between shear walls [2, 3]. The floors are generally considered to be simply supported on the walls below, parallel to the in plane-actions. In conventional light-frame timber floors, continuous 'chords' are fixed at either edge of the floor to act in tension and compression and resist the resulting bending moment [2]. In CLT floors, in contrast, no external chords are used to resist the tension forces due to the bending moment, so the connections to the walls below become fundamental.

In CLT construction, if no connection was used on the supporting walls below, the in-plane bending actions would be transferred simply by the floor-to-floor connections. In reality, there is always a connection between the floor panels and the walls below, even if they are designed as simply supported.

If the floors of a building behave as a flexible diaphragm, then their stiffness affects the load distribution between shear walls under both dynamic [4] and static [5] lateral loading. The flexibility of the floor diaphragm affects structural behaviour in various ways: the load distribution between shear walls is altered [6, 7] and the magnitude of the peak lateral deflection becomes greater than that of the the lateral load resisting system [8]. This subject has been studied for conventional materials used in the floor structures of multi-storey buildings, such as light timber framing [9] and concrete [3]. Chen et al. [6, 7] showed that load distribution on walls depends on the stiffness ratio between floor and walls and that the design method based on envelope forces (*i.e.*, taking the larger of the shear wall forces based on either flexible or rigid diaphragm) may be nonconservative. Accurate calculation of design loads on the lateral load resisting system therefore requires a good prediction of the true diaphragm stiffness.

In concrete diaphragms, analysis based on a strut and tie analogy is recommended [3] and for light timber frame floors design guidance exists [2], but studies of diaphragm deflection in CLT floors are more limited. Pei et al.[10, 11], for example, assume rigid diaphragm behaviour in their designs of a multi-storey CLT apartment.

As is often the case in timber structures, strength and deformation characteristics of diaphragms are strongly dependent on connection behaviour. Typically, adjacent CLT panels at either wall-wall or wall-floor interfaces are connected by screws, and both load-deformation behaviour and ultimate load capacity has been studied for various alignments of screw and panel [12, 13, 14, 15, 16]. Loss and Frangi [17] and Loss et al. [18] investigate in-plane behavior of CLT floors in steel-timber hybrid structures through experimental tests on both connections and full diaphragms, and show significant contributions to deformation from steel-steel, steel-timber and timber-timber connections. In the steel-timber hybrid system, the beams supporting panel edges are taken to act as top and bottom chords transmitting the diaphragm forces.

In studies of structures with CLT forming walls and floors, the capacity of the supporting elements to act as top and bottom chords has generally not been considered. Moroder et al. [19] present a strut-and-tie analysis method for CLT systems. Australian design guidance [20] considers the linear combination of the elements of the deformation of the panel due to elastic deformation of the timber elements and connection slip. This model includes shear and bending deformation in the floor plate, acting as a deep beam, and takes the tension 'chord' to be within the CLT panels. Such an analysis neglects the connection to the supporting panel below.

There have been various experimental studies on complete CLT systems which include floor diaphragms, but most building-scale experimental work does not present measurements of diaphragm flexibility (e.g. [21, 22]). This may be because full-scale building tests are carried out on buildings with relatively small plan areas for practical reasons, for example to fit a shaking table. Popovski and Gavric [23] tested a two-storey CLT structure under lateral load with measurement of diaphragm flexibility. Their floor slab had a length of 6m between shear walls, and was made from three CLT panels. These were connected at either end of the span onto continuous transverse wall panels below. They reported a midspan deflection of the diaphragm of 3.8mm.

In this paper, the effect of each of the connections between CLT panels in a floor diaphragm is considered. Both the connection between adjacent floor panels and between the floor panels and wall panels at the edges are considered, modeling the situation in which the connection to the walls provides a tension chord as the diaphragm bends.

A novel analytical model is presented which concisely describes the in-plane displacements of the CLT floor diaphragms. A numerical model has been used to validate the results of the analytical model. A parametric study has been carried out through the analytical model, investigating the effect of geometric and mechanical properties of the CLT floor panels and the connections between them.

1.1. Contribution

The study presented in the paper offers three major contributions to the field:

1. it describes a new model for the internal distribution of in-plane actions in CLT floors, both in its complete two-dimensional form and in a simplified one-dimensional form;

2. it describes an important additional contributing factor to the response of the floor diaphragm, the connection to the supporting walls below, not included in previous work or design guidance;

3. it presents a sensitivity analysis highlighting the major contributions to the in-plane flexibility of CLT floors.

A simplified equivalent frame model is proposed, which can be used in practice to evaluate the interaction between floor and walls in the distribution of lateral forces between shear walls in a building with CLT floors.

2. Experimental Methods

The experimental methods in this study set out to investigate reasonable bounds for the connection behaviour modeled in the mechanical models described in §3. Data from other researchers provided much of the input required to assess those bounds, but a test series was carried out to investigate the full force-displacement behaviour of a connection, and to evaluate the evolution of stiffness under in-service loading. The tests covered a common form of connection in CLT floor plates: a lap joint with screws through the overlapping timber. The test setup shown in Figure 1 was used, permitting both tension and compression loading on a symmetrical pair of lap joints.

The CLT panels tested were 85mm thick, made up of five 17mm layers, with the lap joints 50mm wide. The screws used were Simpson Strong-tie®Eurotec 8.0×80 screws, with an inner thread diameter of 6mm, an outer thread diameter of 8mm and a length of 80mm. These are the same screw dimensions used by Gavric et al. [12], although they are from a different manufacturer. The moisture content of each specimen was measured on each face by electrical resistance after testing, giving an overall mean of 10.6% and a coefficient of variation of 8.5%. The density was measured for each specimen and, corrected for 12% moisture content, had a mean of 448kg/m^3 and a coefficient of variation of 1.5%. 12 specimens were tested.

These experiments were designed to supplement the information available in the literature and give further insight into the nature of the force-displacement response of this form of connection. The lapped screw joint specimens were tested under cyclic loads of 20% and 40% of their characteristic load calculated according to Eurocode 5 [24], giving a range of applied force representative of in-service loading. In dowel-type connections, for one-sided loads, the stiffness under unloading and reloading is higher than that under initial load, as the uneven surface of the timber at the hole edge, and some of the timber in the area of stress concentration close to the hole edge, deforms plastically [25, 26]. Pilot tests at 20% of the characteristic load showed a small further increase in that stiffness, so further cycles of load were applied to investigate whether the effect was substantially complete after the first cycle of load, or whether there would be a continued change in shape of the force-displacement diagram with further cycles of load.

As indicated in Figure 1, the displacement was measured as the mean of two readings taken by linear displacement transducers fixed on either side of the central piece of CLT.

3. Mechanical models for the in-plane behavior of a CLT floor

The mechanical behavior of a rectangular CLT floor, supported on four edges and subjected to a uniform distributed horizontal load, is analyzed in this section by means of two different mechanical models: a 2-D plane model (PM) and an equivalent frame model (EFM). The geometrical and mechanical properties of CLT panels, the properties of mechanical connections and the boundary conditions are defined in this section.

3.1. The Plane Model - PM

Consider a rectangular CLT floor composed of m panels with length b and subjected to an in-plane uniform horizontal load q as seen in Figure 2 . The floor span and total width of floor are L and B, respectively, where B is equal to $b \times m$. The CLT panels are characterized by odd number of orthogonal layers with a total thickness equal to t. The total thickness of longitudinal and transversal layers is assumed equal to t_L and t_T, respectively. The modulus of elasticity and the shear modulus of wood each layer are defined as E_0 and G.

In the PM mechanical model CLT panels are considered as 2D in-plane stress homogeneous elements (membrane 2D elements) characterized by an elastic-linear orthotropic behavior, [27]. Since the modulus of elasticity of timber parallel to grain is much larger than that perpendicular to grain, the moduli $E_{eq,L}$ and $E_{eq,T}$ in the Longitudinal (L) and Transversal (T) directions are defined according to composite theory [28] by Eq. 1 and Eq. 2.

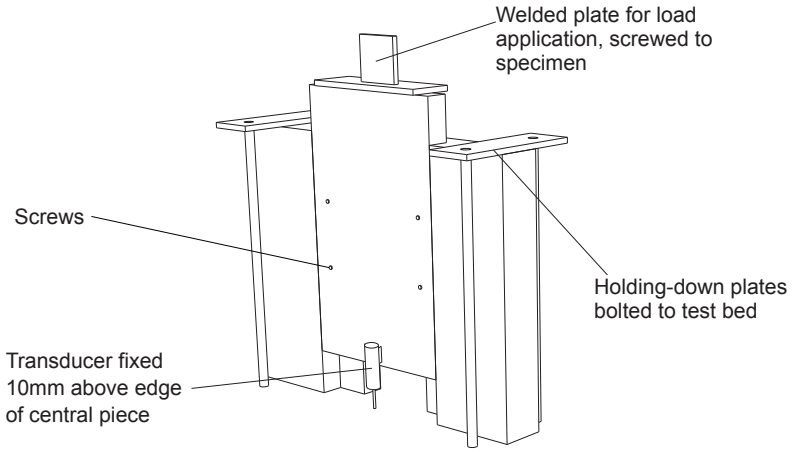

Fig. 1. Test setup for lap joint between adjacent CLT panels with screws.

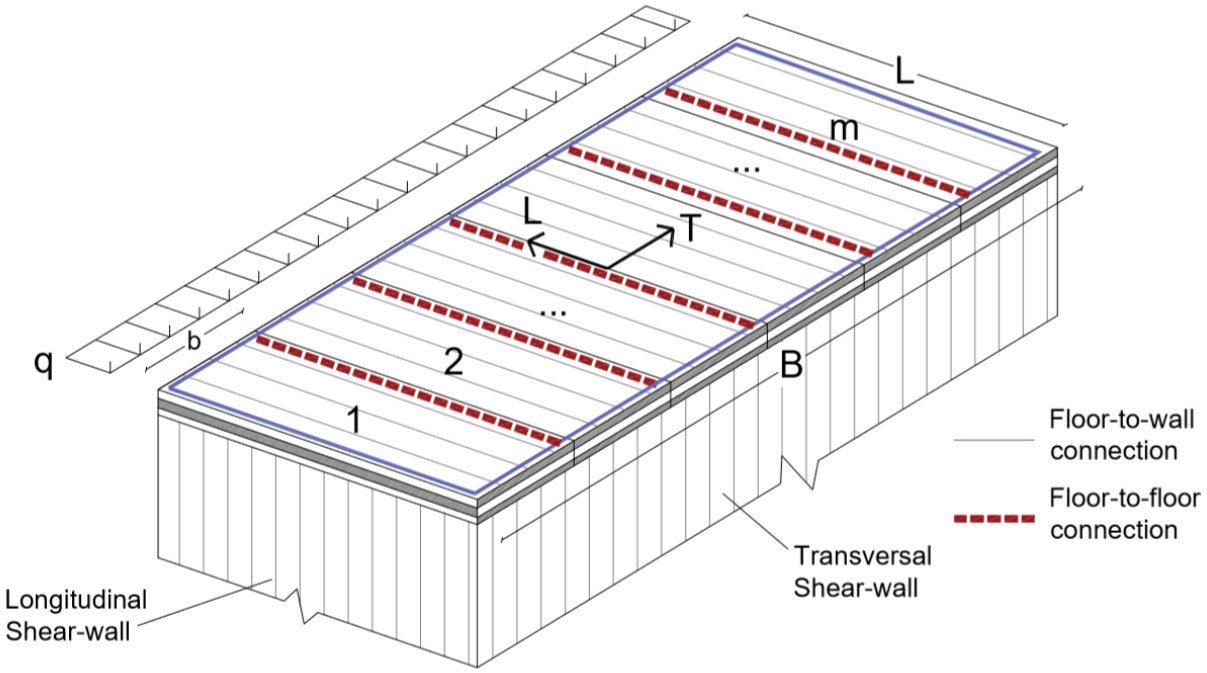

Fig. 2. The PM model.

$$E_{eq,L} = \frac{E_0 \cdot t_L}{t} \quad (1)$$

$$E_{eq,T} = \frac{E_0 \cdot t_T}{t} \quad (2)$$

An equivalent shear modulus G_{eq} which takes into account the number of layers, the total thickness of the panels and the width of boards is considered as proposed by Brandner et al. [29].

Figure 3 shows the connection stiffnesses in the PM. The connection between adjacent floor panels, the floor-to-floor connection, is represented by line springs with an elastic stiffness per unit length in the direction parallel to the panels (the L direction) equal to $K_{f-f,L}$. Transverse to the panels (in the T direction) the stiffness per unit length of the line springs is equal to $K_{f-f,T}$. The connections to the vertical structure (the floor-to-wall connections) are represented by line springs acting only in the direction parallel to the edges of the floor with a stiffness per unit length equal to K_{f-w}.

The stiffness in the orthogonal direction to the edge of the floor is assumed equal to zero, since the vertical supporting elements are not in general designed to withstand any lateral load out of their own plane Izzi et al. [27]. Mechanical connections at the base are designed only to resist the in-plane racking load CEN [30]. The walls can, therefore, be assumed as hinged at the base for lateral loads acting out-of-plane. The vertical supporting elements are in this study located only along the four edges of the floor and no internal walls are considered. Further studies will be performed in the future to investigate the role of connections along internal walls.

The behavior of CLT panels and connections is assumed to be linear elastic with the only exception the floor-to-floor connection in the T direction. In order to take into account the interaction between two adjacent floor panels, different values of stiffness $K_{f-f,T}$ are used when the line spring works in tension or compression. When the two adjacent panels separate the stiffness of the spring is related to the stiffness of the floor-to-floor mechanical connection, whereas when the panels contact each other, a rigid contact element is adopted. As a results, the mechanical behavior of the floor-to-floor connection in the T direction is modeled by elastic non-linear links with linear elastic behavior in tension $K^{+}_{f-f,T}$ and rigid behavior in compression $K^{-}_{f-f,T}$. The same assumption is commonly adopted in the modelling of hold-down anchors: to simulate the contact of the wall with the ground, a higher stiffness is assigned to the hold-down in compression, giving non-linear elastic behaviour Izzi et al. [27].

The external load q is transferred through the floor panels to the two longitudinal shear-walls. Thinking the floor panels as a deep beam, their deformation can be split into 'shear' and 'bending' contributions. The floor displacement due to shear, Δ_S, is hence related to: *i)* the in-plane shear deformation of the j^{th} panel $\Delta_{G,j}$, depending on the equivalent shear modulus G_{eq} and the total thickness t of the panel, *ii)* the contribution $\Delta_{f-f,L,j}$ of the floor-to-floor connection along the L direction between the j^{th} and $j+1^{th}$ panel and *iii)* the contribution Δ_{f-w} due to the floor-to-wall connections, along the longitudinal walls.

The displacement due to bending, Δ_B, is dependent on: *iv)* the in-plane bending stiffness of the CLT panels due to the equivalent modulus of elasticity $E_{eq,T}$ and total thickness t of the panel, *v)* the stiffness of the floor–to-floor connections along the T direction, *vi)* the stiffness of the floor-to-wall connections along the transversal shear walls. If contributions *iv)* and *v)* represent internal boundaries to ensure the in-plane continuity of the floor, the floor-to-wall connections along the transversal shear-walls *vi)* are defined as external flexible restraints, limiting the rigid rotation of the panels. This represents an important additional contributing factor to the response of the floor diaphragm, not included in previous research or design guidance.

The non-linearity of the floor-to-floor connection along the T direction is novel, and is analyzed in the sensitivity analyses in the following sections. The analyses show that the contact length between the panels, l_{cont}, is significantly lower than the length which would be obtained assuming the same stiffness in compression and tension. The rigid contact means the panels rotate so that the relative transversal displacement on the compression edge is significantly lower than the displacement on the tension edge. If the same stiffness were assumed in both compression and tension, the panels would rotate with overlap in the compressive zone, giving an unrealistic panel deformation.

In order to facilitate the representation of results obtained from sensitivity analyses, a spring model can be defined for the in-plane behaviour of CLT diaphragms. Each contribution *i)* to *vi)* is represented by equivalent horizontal spring, working in-parallel or in-series in an equivalent spring system as shown in Figure 5.

Firstly, the global in-plane behaviour of the CLT floor is schematized considering the shear and bending deformation contributions as uncoupled. As a result the global deformation of the floor can be obtained simply summing the displacement due to the bending with the displacement due to shear deformation. Secondly, the shear contribution, Δ_S, can be represented by three in-

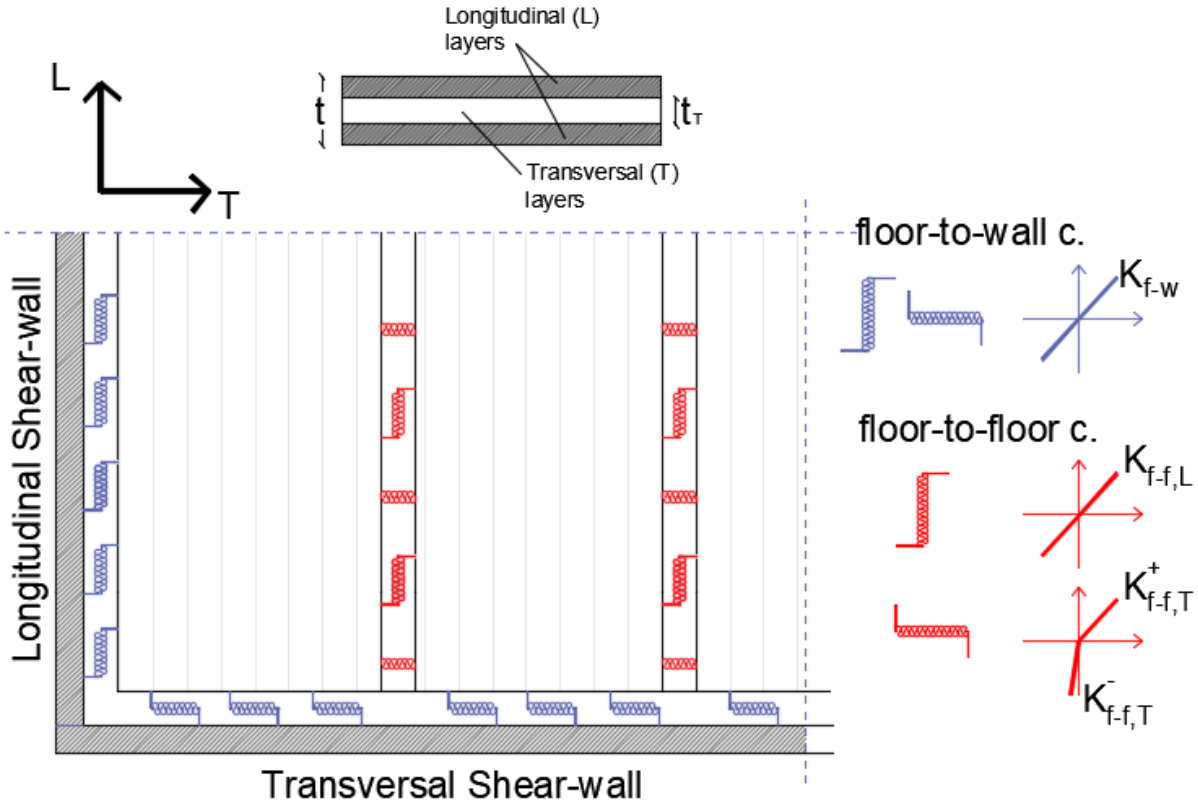

Fig. 3. Mechanical properties of connections in the PM model.

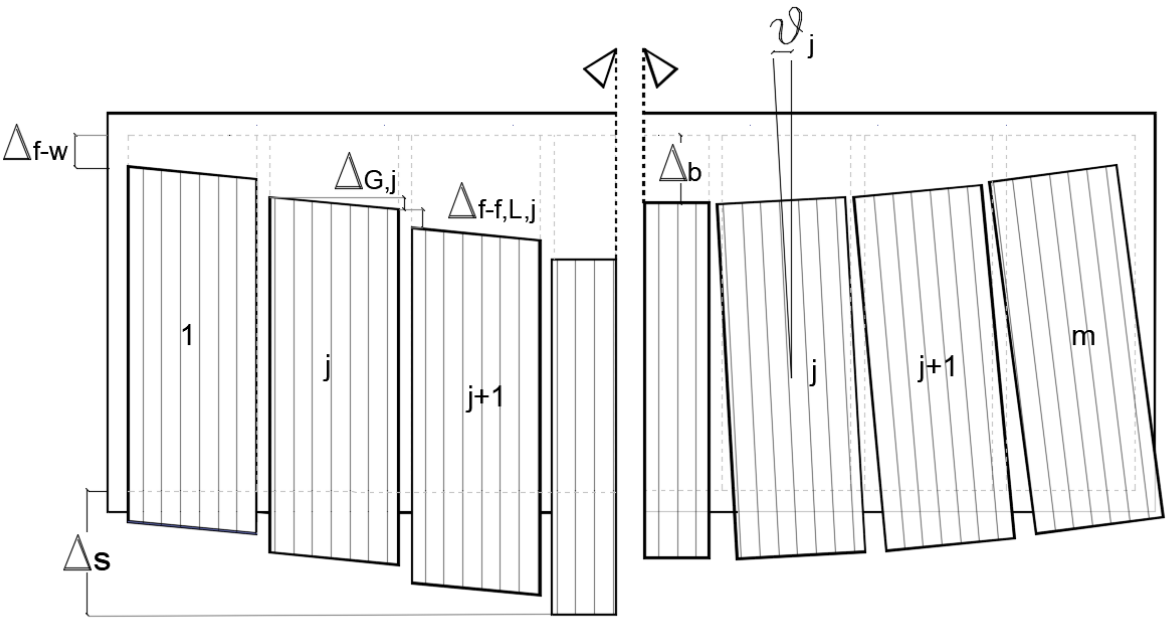

Fig. 4. Deformation contributions due to shear and bending.

series springs accounting for the shear deformations in the panels *i)*, floor-to-floor *ii)* and floor-to-wall connections *iii)*. The floor displacement due to bending, Δ_B, is schematised by two springs in series, accounting for the bending contribution of the panels *iv)* and floor-to-floor connections *v)*, in parallel with a single spring which allows for the floor-to-wall *vi)* bending.

3.2. The Equivalent Frame Model - EFM

In the equivalent frame model (EFM), the CLT panels are represented by equivalent frame elements of length b with cross section $t \times L$. The modulus of elasticity and shear modulus are equal to $E_{eq,T}$ and G_{eq}. Continuity of the frame elements comes from the two internal springs shown in Figure 6: the rotational springs $k_{rot,f-f}$ representing the in-plane bending contribution of the floor-to-floor connection in the T direction, contribution *v)*, and a transversal spring $k_{s,f-f}$ which takes into account the shear deformation due to the floor-to-floor connection in the L direction, contribution *ii)*. The floor-to-wall connections along the longitudinal shear walls, contribution *iii)*, are modeled with two external transversal springs $k_{s,w-f}$ and the rotational boundary due to the floor-to-wall connections along the transversal shear walls, contribution *vi)*, is represented by external rotation springs $k_{rot,f-w}$ located in the center of each frame element.

The shear diagram due to the external load q is the same as a simply supported continuous beam of length B with rigid supports as shown in Figure 6 a).

The bending moment diagram, on the other hand, can have a different magnitude and shape. The two limit cases are represented by a value of the rotational stiffness $k_{rot,f-w}$ equal to zero (*i.e.* stiff beam, flexible floor-to-wall connection, see Figure 6 b) or to infinity (*i.e.* flexible beam, stiff floor-to-wall connection, see Figure 6 c).

The internal and external spring stiffnesses for the EFM are defined as a function of the geometrical properties of the panels and the value of stiffness of the line springs in the plane model. For the external and internal transversal springs, a uniform stiffness distribution along the panels is assumed, so that $k_{s,f-f}$ and $k_{s,f-w}$ are defined as in Eq. (3) and Eq. (4).

$$k_{s,f-f} = K_{f-f,L} \cdot L \tag{3}$$

$$k_{s,f-w} = K_{f-w} \cdot L \tag{4}$$

The stiffness of rotational springs is defined assuming a length of contact between the panels, l_{cont}, equal to 10% of the floor length, as in Figure 7. This value is commonly suggested for CLT walls in contact with the ground when subjected to a rocking moment, due to the higher flexibility of the hold-down anchors in

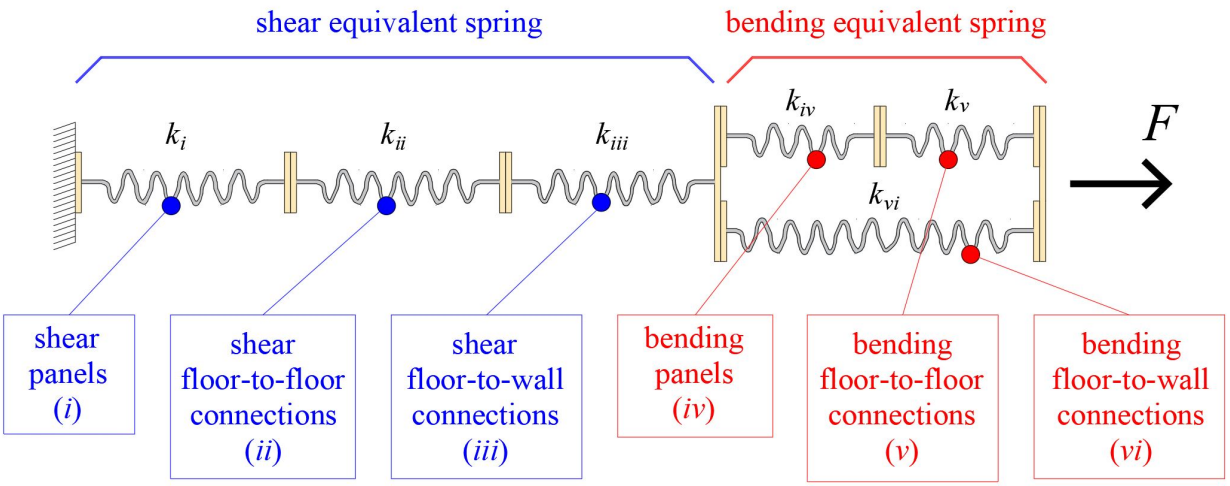

Fig. 5. Spring model for the in-plane behaviour of CLT diaphragms.

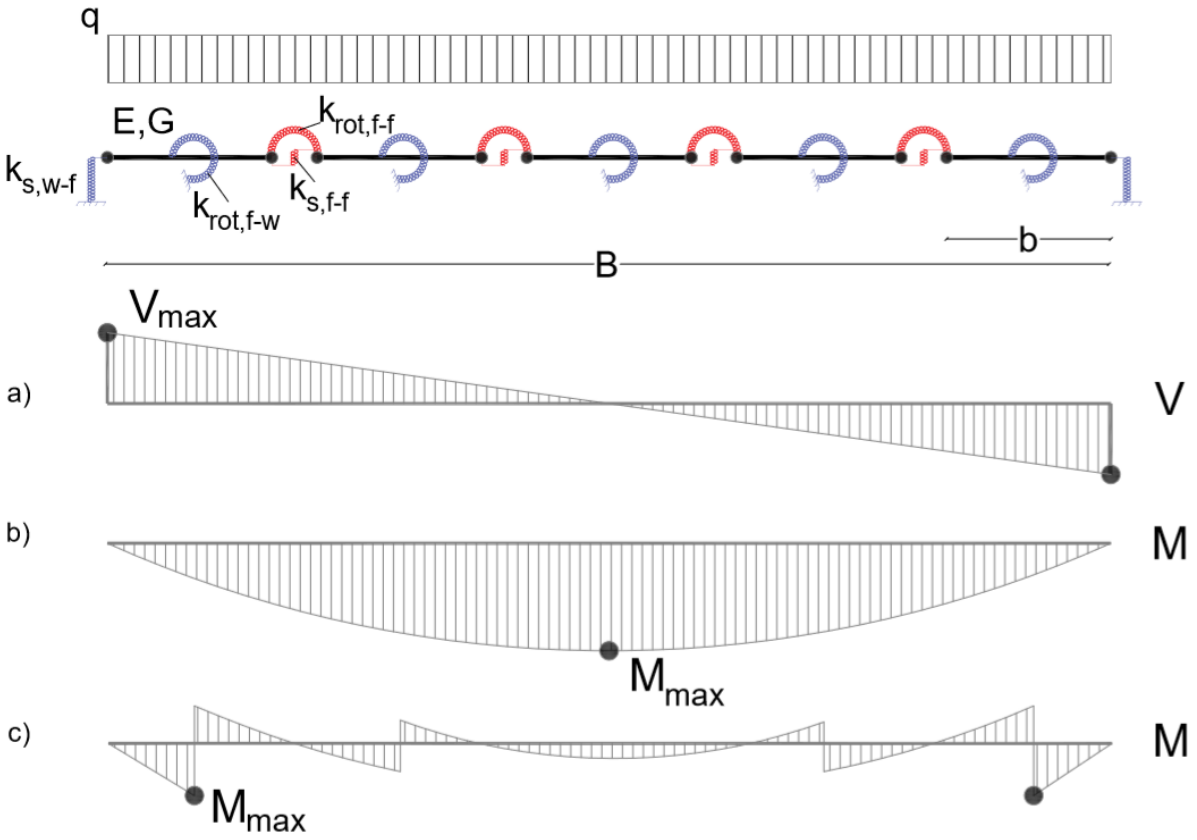

Fig. 6. Internal actions in the EFM model a) shear, b) bending in case of flexible floor-to-wall connection, and c) bending in case of stiff floor-to-wall connection.

tension zone than the contact between the wall and the ground, see for example [31] and [32]. The external rotational spring stiffness is hence calculated taking into account the product of the line spring stiffness along the transversal shear-walls and the internal level arms according to Eq. 5.

$$k_{rot,f-w} = K_{f-w} \cdot b \cdot l_{cont}^2 + K_{f-w} \cdot b \cdot (L - l_{cont})^2 \quad (5)$$

Similarly, the internal rotational spring stiffness is obtained integrating the rotational stiffness due to the line spring with respect to the transversal direction, as in Eq. (6).

$$k_{rot,f-f} = K_{f-f,T}^{-} \cdot \frac{l_{cont}^3}{3} + K_{f-f,T}^{+} \cdot \frac{(L - l_{cont})^3}{3} \quad (6)$$

The stiffness $K_{f-f,T}^{+}$ represents the transversal stiffness of the floor-to-floor connection in the T direction. $K_{f-f,T}^{-}$ takes into account the rigid contact between the panels and the transversal compression of the panels per unit length, according to Eq. 7.

$$K_{f-f,T}^{-} = E_{eq,T} \cdot \frac{t}{b} \quad (7)$$

3.3. Validation of the Equivalent Frame Model

The validation of the EFM was carried out analyzing the in-plane lateral deformation of 15 different floors, changing geometrical and mechanical properties, by means of Finite Element Models. Each floor has been modelled according to the EFM and the 2D model and the maximum lateral displacement in the center of the floor between the PM and EFM models was compared.

For the PM model, the CLT panels were modeled with 2D in-plane stress elements for an elastic linear equivalent orthotropic material with a total thickness t. The moduli in the L and T directions were $E_{eq,L}$ and $E_{eq,T}$, whereas the shear modulus was taken equal to G_{eq}. 1-point linear springs were adopted to represent the floor-to-wall connections and link elements were used for the floor-to-floor connections. Because of symmetry, only half the floor was modeled, with lateral restraints along the line of symmetry. For the EFM model, frame elements with a rectangular section $t \times L$ were used for the CLT panels, whereas linear spring and link elements were adopted both for the rotational and transversal springs. 1-point linear spring elements were used for the external springs, *i.e.* the floor-to-wall connections and 2-point links for the internal springs, *i.e.* the floor-to-floor connections.

The floors analysed had a span length L of 4m, panel length l of 2m, modulus of elasticity E_0 of 12000MPa and equivalent shear modulus G_{eq}, 500MPa. Three different values of width B equal to 6, 10 and 18 m were selected with a total thickenss of 100 and 180mm. For the floor-to-wall stiffness K_{f-w} three values, equal to 2, 40 and 200 N/mm^2, were chosen whereas a constant value of $K_{f-f,L}$ equal to 2N/mm^2 was used.

Three different groups of case studied were considerer for this purpose: *a)* shear deformation neglected, *b)* in-plane bending neglected, *c)* shear and the in-plane bending considered. When the bending deformation contribution is zero (case b), the EFM has errors lower than 3%. When the shear deformation contribution is zero (case a), there are errors in terms of maximum lateral displacment of up to 15%, primarily because the EFM model cannot capture the elastic-rigid contact behaviour between the panels. In case c), the maximum error is lower than 5%. Nonetheless, the EFM is considered to provide a reasonable degree of accuracy with very low computational cost, enabling a broad sensitivity study.

4. Results and Discussion

4.1. Connection tests

The force-displacement diagrams in Figure 8 are typical, and show the highly hysteretic behaviour of this type of connection. The shape of the force-displacement diagram is typical of a frictional elastic system, where a frictional force must be overcome in order to change the direction of movement. Therefore, at the left- and right-hand sides of the force-displacement loop, there is a substantial change in force, with little change in displacement. This high stiffness while friction is limiting is also evident in the unload-reload cycle marked with + in plot a), in which friction is never overcome. The very first loading, marked with * in plot a), starts at a stiffness close to that for limiting friction, and tends towards the elastic stiffness. Plot b) shows that the cyclic behaviour is relatively consistent over the 1000 cycles of force applied: although there is a change in stiffness in the first 10 cycles of load applied, the magnitude of the change is below 10% and there is no substantial continued change over the further cycles up to 1000. It thus appears that the stiffness measured on the first unload-reload cycle is a reasonable estimate of the stiffness after many cycles of serviceability loads. In plot c), it can be seen that a higher applied load leads to more deformation in the elastic (as opposed to the frictional) regime, and a lower overall stiffness.

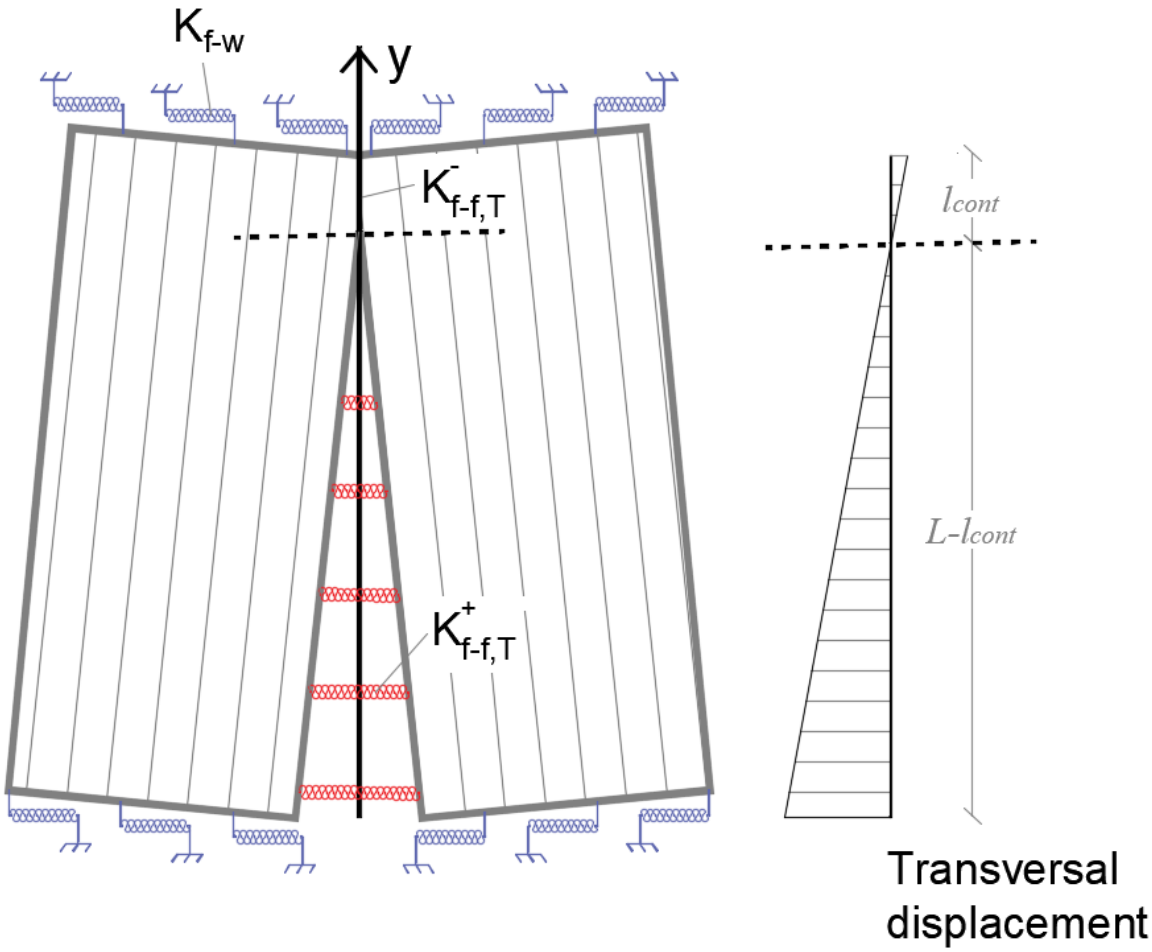

Fig. 7. Floor-to-floor transversal displacement.

Various equivalent elastic stiffnesses could be defined for this force-displacement response: Figure 8 shows a stiffness for limiting friction, a stiffness for the elastic regime once friction is overcome and a secant stiffness for a cycle of load. Plots c) and d) show little change in any of these stiffnesses over the 1000 cycles of applied force.

Figure 9 indicates the range of stiffnesses reported in the literature for joints between adjacent CLT panels [14, 15, 12], along with the experimental results from this study. For comparison with other studies, the 'elastic regime' stiffness illustrated in Figure 8 was used for the experimental work in this study. Gavric et al. [12] also measure the stiffness of screwed connections between CLT panels in cyclic tests, using the points at 10% and 40% of the estimated failure load to evaluate the stiffness according to EN 12512 [33]. Loss et al. [14] use the EN 12512 method [33], but applied to a monotonic test. The initial loading curve in Figure 8 is stiffer than the elastic portion in subsequent cycles, and this may partly explain the higher stiffnesses recorded by Loss et al. [14], although this may also be due to the longer embedment length and larger diameter screws used compared with Gavric et al. [12]. Hossain et al. [15] present the stiffness calculated both from monotonic and cyclic loading tests. The difference between the stiffnesses measured by each method varies for the different specimen configurations, but can be as high as a factor of two. This correlates well with Figure 8 (a).

Figure 9 (a) shows the stiffness of an individual connector, and (b) the maximum stiffness per unit length of joint, if the connectors were spaced at their minimum spacing. There is a very substantial scatter in the results, and no clear trends in stiffness with either screw diameter or embedded length. There is, however a clear indication that inclined screws are stiffer per connector.

Figure 9 (c) and (d) presents results from literature for connections between orthogonal panels (e.g. wall-to-floor connections). Once again, the higher stiffness of inclined screws per connector is evident.

All these results are for connections in their 'elastic' range (although as shown in Figure 8 this range includes elastic and frictional behaviour). At higher loads, when fasteners yield, a reduction in stiffness would be expected, but this study focuses on modelling the floor behaviour in the elastic range.

Inclined screw connections give the highest stiffness for an individual connector, and may, therefore, give the most economical connections. The highest stiffness connection, however, in terms of stiffness per metre run with the minimum connector spacing, comes from screws without inclination, since they can be placed at a closer spacing. The range of stiffnesses per metre run in the literature cover an order of magnitude difference from lower than 10 N/mm^2 up to over 100 N/mm^2. Connectors would not necessarily be placed at their minimum spacing, and so a range of stiffness from 1 N/mm^2 to 100 N/mm^2 is used for the sensitivity analysis presented here. In fact, since these connections are generally designed to resist low forces, and have large connector spacing to reduce the labour required on site, the most likely values in construction are between 1N/mm^2 and 10 N/mm^2. Values of 100 N/mm^2 are unlikely in practice.

4.2. Sensitivity analysis

The in-plane deformability of CLT floor diaphragms was studied through a sensitivity analysis using the EFM, with the aim to understand the main mechanical and geometrical parameters which affect the in-plane behaviour.

The sensitivity analysis was carried out considering different values of the geometrical and mechanical parameters. The chosen values vary within appropriate ranges to cover the typical values which would be expected in practice. For the CLT panels a modulus of elasticity of the timber E_0 of 12000MPa, and an equivalent shear modulus G_{eq} of 500MPa were chosen. A ratio of the thickness of the layers in the transversal direction t_T and total thickness t of the panels equal to 0.33 was fixed, giving an elastic modulus in the transversal direction $E_{eq,T}$ of 4000MPa according to Eq. (1). A panel width b of 2m and a span L of 5m were considered. The width B and the total thickness t of the floor were varied as follows: B = [6 10 14 18 22]m; t = [100 140 180 220]mm.

The elastic stiffnesses per unit length of line springs representing floor-to-wall, K_{f-w}, and floor-to-floor, $K_{f-f,L}$ and $K_{f-f,T}$, connections were varied between 1N/mm^2 to 100 N/mm^2 as follows: K_{f-w} = [1 10 100]N/mm^2; $K_{f-f,L}$ = [1 10 100]N/mm^2; $K_{f-f,T}$ = [1 10 100]N/mm^2. The values of stiffness per unit length 1-10-100 N/mm^2 have been labeled Low-Medium-High in the following analysis and discussion.

Since the stiffness in the transversal direction $K_{f-f,T}$ can be equal or lower than that in the longitudinal direction $K_{f-f,L}$, depending by the type of the connection system, two cases were analysed in the sensitivity analysis. First, Case A where the stiffness in longitudinal and transversal directions have the same values and second, Case B where the stiffness in the longitudinal direction varies from 1 to 100N/mm^2, while the the stiffness in the transversal direction is set to 1N/mm^2. In this section

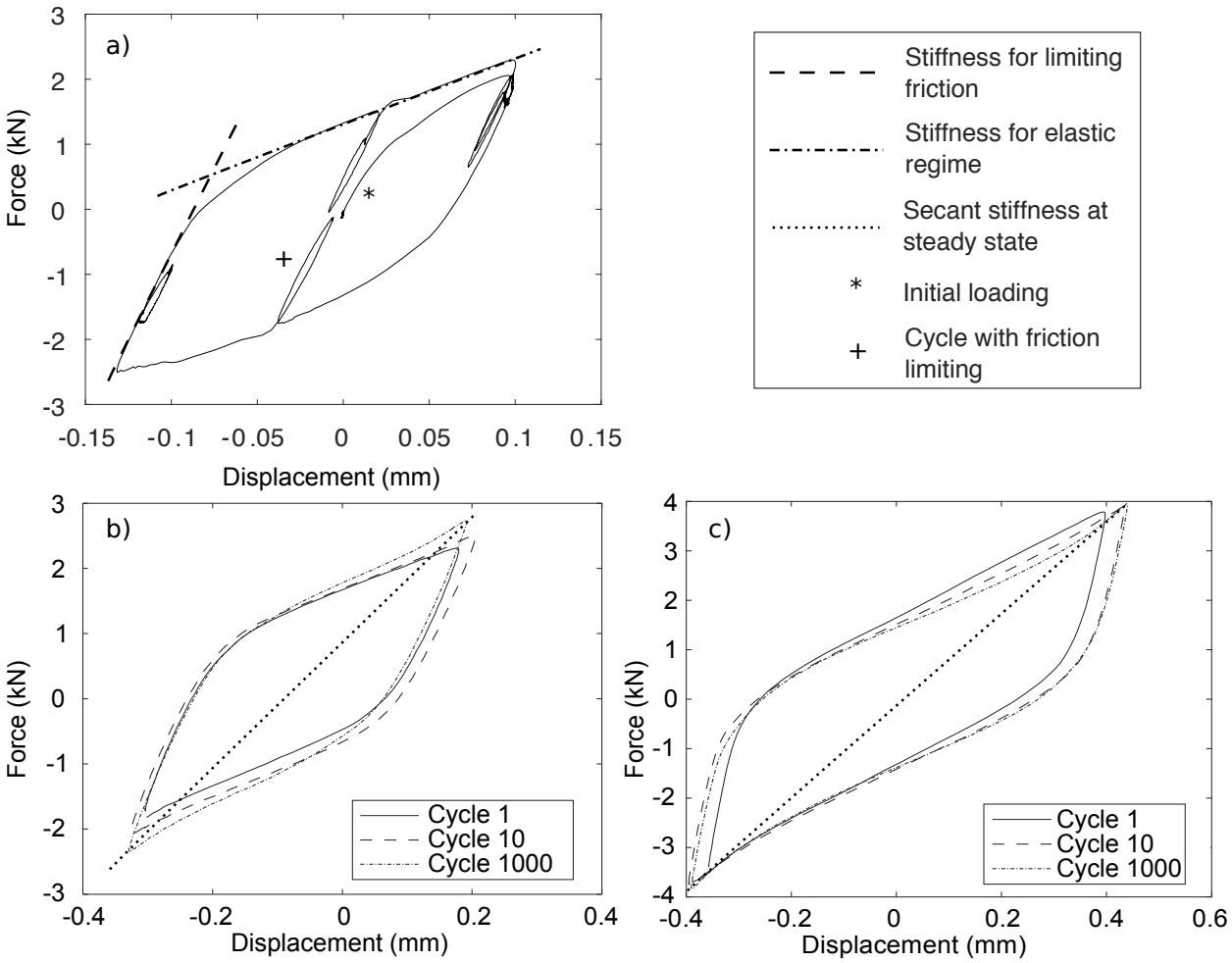

Fig. 8. a) The initial loading and first cycle of load on a screwed lap joint, b) Force-displacement diagrams under fully-reversed cyclic loading with peak values of 20%, c) 40% of its characteristic ultimate force.

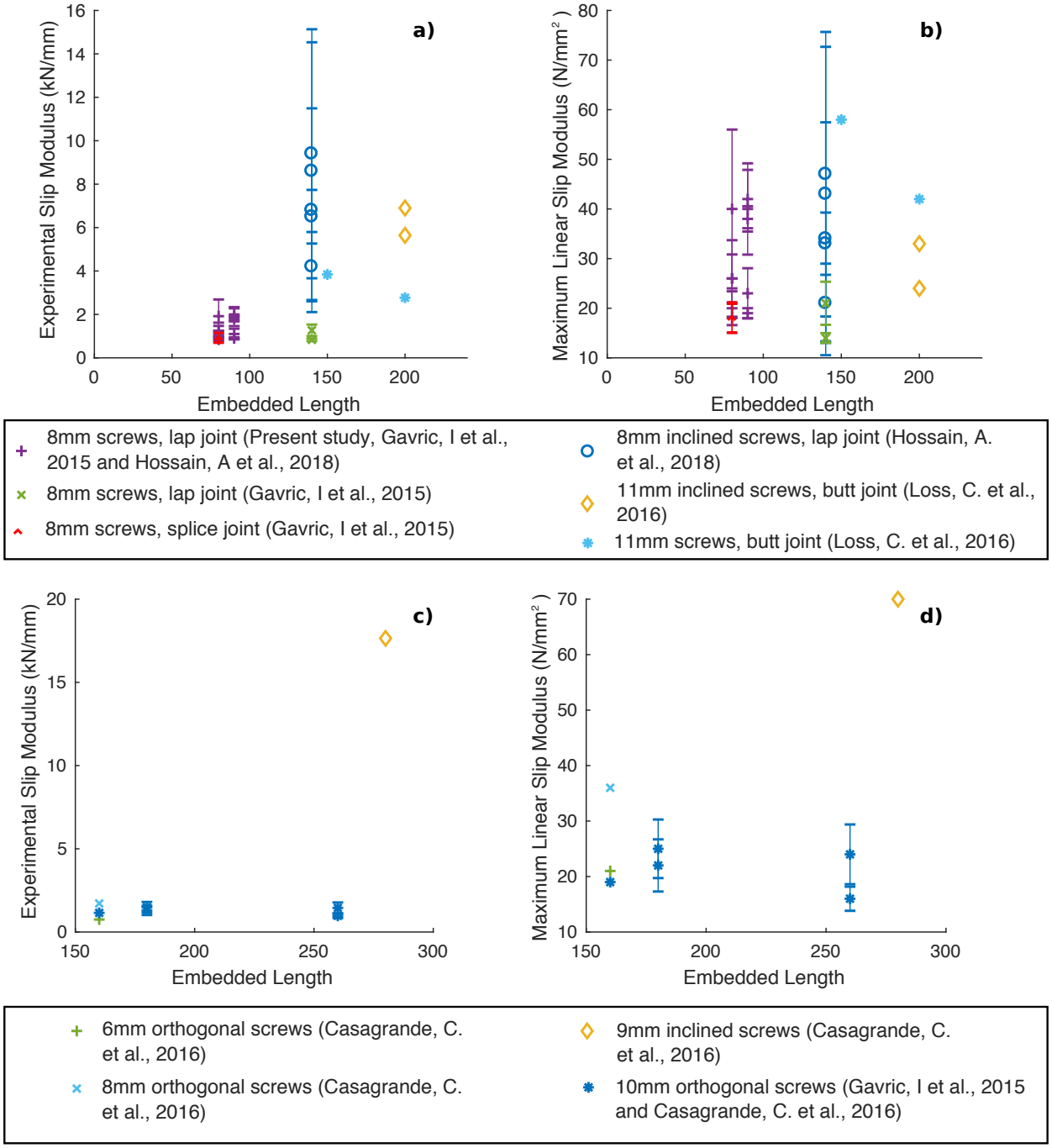

Fig. 9. Stiffness of connections between adjacent panels a) per connector, and b) per metre length at the closest allowable spacing) and between orthogonal panels c) per connector, and d) per metre length at the closest allowable spacing). Error bars show standard deviation where reported.

only the results of Case A are reported. The results of Case B are reported in a final appendix.

The results of the sensitivity analysis are reported in graphs organised in matrix form, where the position of the axes depends on the values of stiffness per unit of length of the floor-to-wall and floor-to-floor connections. The position in the matrix is referred to from here on with the row first, representing the floor to floor connection stiffness and the column second representing the floor-to-wall connection stiffness. So High-Low, for example, refers to a combination of High floor-to-floor stiffness and Low floor-to-wall stiffness, at the bottom left of of the matrix.

First, the in-plane flexibility of the floor was analysed varying the thickness t and width of the floor B. The in-plane flexibility of the floor $\tilde{\Delta}$ was defined as the ratio between the total maximum displacement Δ and the distributed load q. The results of thickness analysis are shown in Figure 10.

Note that the in-plane flexibility $\tilde{\Delta}$ varies strongly with the width of the floor B and the stiffness per unit length $K_{f-f,L}$, $K_{f-f,T}$ and K_{f-w}. The maximum and minimum values of $\tilde{\Delta}$ are 10.2 mm^2/N and 0.21 mm^2/N for B equal to 22 m and 0.92 mm^2/N and 0.02 mm^2/N for B equal to 6 m. A factor of 50 variation is therefore evident for both widths B.

Figure 10 also shows the percentage variation of $\tilde{\Delta}$ of both thickness 100mm and 220mm respect to the thickness 140mm. It can be observed that the sensitivity to thickness increases with an increase in stiffness per unit of length of the connections: in the High-High condition, the peak variations are 26% and -23%. The sensitivity is much lower for the Low-Low condition with variations of 1% and -1%. However, if only Low and Medium connection stiffnesses are considered, which represent more common situations of practical constructions, the maximum variation is 6%. Even excluding only the High-High condition, the greatest variation is 13%.

The results in §4.1 showed that a stiffness of 10N/mm^2 is exceeded when connectors are placed at their minimum spacing, but it is considered that this would be very rare in practice. It is likely, therefore, that the High condition is very rarely reached, and so the influence of the variation of the thickness in the in-plane flexibility is below 6%. On this basis, the following analyses were carried out considering only the thickness of 140mm in order to reduce the variables involved.

The next analysis investigated the displacements due to shear and bending deformations. The contribution of each was evaluated as the ratio between shear or bending maximum displacement and the total maximum displacement: Δ_S/Δ and Δ_B/Δ. Figure 11 show this analysis.

Note that shear is the major contribution for all cases. It ranges between 99.3% and 59.9%. The high shear contribution in this study is due to the low aspect ratio of the floors, between 1.2 and 4.4.

It can be noticed that when the K_{f-w} increases, the bending contribution decreases in almost all cases, with a few exceptions. The most marked exception is switching from High-Low to High-Medium conditions where the bending contribution increases for all B. In general, increasing the stiffness per unit of length of the floor-to-wall connections stiffens the floor in bending.

Similarly, when the $K_{f-f,L}$ increases, the bending contribution increases in almost all cases. The most marked exception is switching from Medium-Low to High-Low conditions where the bending contribution decreases for all B analysed.

Since the displacement due to shear deformation is schematized as three springs in series, it is possible to asses the separate contributions of the panels, floor-to-floor and floor-to-wall connections to shear displacement. They were evaluated considering the ratio between the shear displacement contributions *i)*, *ii)* and *iii)* and the total displacement, shown in Figure 11.

Note that when either stiffness per unit of length $K_{f-f,L}$, $K_{f-f,T}$ or K_{f-w} is Low the shear contribution due to the panels is always lower than 6%. The greatest shear contribution in the panels is in the High-High condition, when the floor width B is equal to 22m, at 62,4%. However for values of $K_{f-f,L}$, $K_{f-f,T}$ and K_{f-w} up to 10 N/mm^2, which represents more common situations in practical construction, the shear contribution in the panels is always less than 15%. It is important to highlight that when the shear contribution of the panels is high it means that the thickness of the panels has a greater effect, as shown in High-High condition of Figure 10.

When the width of the floor B increases, the floor-to-wall shear contribution decreases, but the floor-to-floor shear contribution increases. This is because of the increase in the number of joints in the floor, the most flexible part of the system. When $K_{f-f,L}$ and $K_{f-f,T}$ increase, the floor-to-wall shear contribution increases and when K_{f-w} increases the floor-to-wall shear contribution decreases. The greatest floor-to-floor shear contributions is in the Low-High condition, for B equal to 22m and it is 95.6%. As noted earlier, the maximum floor-to-floor shear contribution occurs at maximum B. The greatest floor-to-wall shear contribution is in the High-Low condition, for B equal to 6m and it is 96.7%. Anyway for values of both $K_{f-f,L}$, $K_{f-f,T}$ and K_{f-w} up to 10 N/mm^2, i.e. in more common situations of practical construction, the shear contribution due to the con-

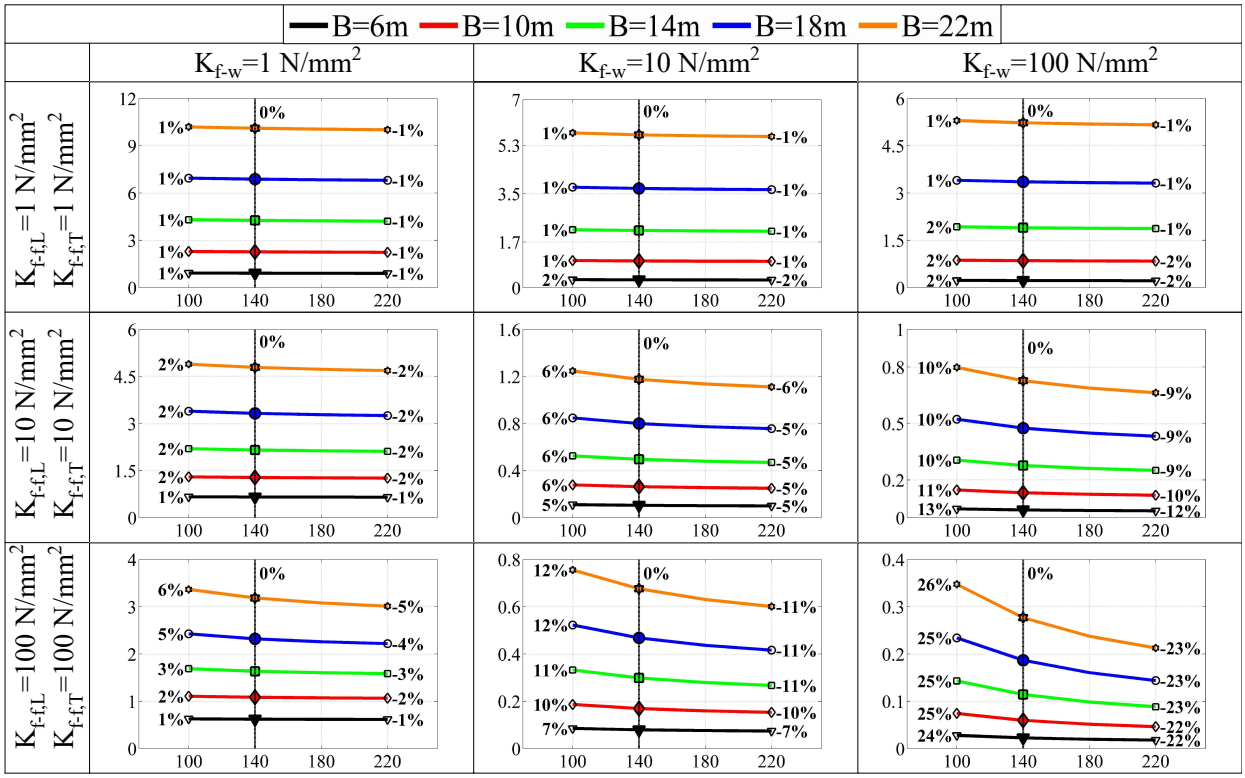

Fig. 10. In-plane flexibility $\tilde{\Delta}[\frac{mm^2}{N}]$ plotted against panel thickness $t[mm]$, Case A ($K_{ff,L} = K_{ff,T}$).

nections ranges between 56.3% and 91.8%. This result shows that the main contributing factor to the in-plane deformation is the connections.

Since the springs representing bending displacement are in parallel, they must be studied in terms of the stiffness contribution, rather than displacement. Considering Figure 5 without the shear equivalent spring, the displacement due to bending deformations Δ_B can be evaluated by Eq. 8. Similarly, the displacement due to bending without the floor-to-wall contribution, Δ_B^*, can be evaluated by Eq. 9, neglecting k_{vi}. The relative contribution of the floor-to-wall and floor-to-floor connections $\tilde{k}_B$ was evaluated considering the ratio between Δ_B and Δ_B^* (Eq. 10).

$$\Delta_B = \frac{F}{k_{iv,v} + k_{vi}} \tag{8}$$

$$\Delta_B^* = \frac{F}{k_{iv,v}} \tag{9}$$

$$\tilde{k}_B = \frac{k_{vi}}{k_{iv,v}} = \frac{\Delta_B^*}{\Delta_B} - 1 \tag{10}$$

where

$$\frac{1}{k_{iv,v}} = \frac{1}{k_{iv}} + \frac{1}{k_v} \tag{11}$$

Figure 12 shows that the $\tilde{k}_B$ parameter varies greatly, between 0.01 and 1000. The maximum value is for the Low-High condition with a floor width of 22m. This is the same condition which has the peak shear floor-to-floor contribution (Figures 11). The minimum $\tilde{k}_B$ value is for the High-Low condition with a 6m floor width. It is interesting to notice that the maximum and minimum $\tilde{k}_B$ values occur where the ratio between the stiffness per unit of length K_{f-w} and $K_{f-f,T}$ is maximum or minimum. It can be seen also that $\tilde{k}_B$ grows as the width of the floor B increases, highlighting the greater stiffening contribution of wall-to-floor connections in comparison with floor-to-floor connections. Finally it can be seen that for values of $K_{f-f,L}$, $K_{f-f,T}$ and K_{f-w} up to 10 N/mm^2, i.e. in more common practical situations, the $\tilde{k}_B$ ranges between 0.1 and 100, varying greatly with floor width and connection stiffness.

4.3. Effects of external rotational springs

The floor-to-wall connections, working as external rotational springs, affect the displacement of the floor and the distribution of internal forces. When their stiffness is zero, the floor is a simply supported beam in bending.

To investigate the magnitude of this effect, an analysis was carried out of the ratio between the displacement of the EFM with, Δ, and without, Δ^*, the external rotational springs. The results are shown in Figure 13 for the same mechanical and geometrical properties used in the previous sensitivity analysis. It can be seen that the ratio $\frac{\Delta^*}{\Delta}$ varies between 1 and 8,as the external rotational springs reduce the displacements compared with the simply supported beam scheme. The ratio $\frac{\Delta^*}{\Delta}$ increases with floor width B, except in the High-Low condition, where the stiffening due to the internal rotational springs is greater than the external ones. This is also shown in the low values of $\tilde{k}_b$ in this High-Low condition (Figure 12). Considering only Low and Medium values of stiffness per unit of length, more common in practice, the ratio $\frac{\Delta^*}{\Delta}$ ranges between 1 and 5.3. This range highlights the substantial effect of the floor-to-wall connections on the displacements.

As described in §3, floor-to-wall connections change the shape of the bending moment diagram (see Figure 6), reducing the maximum moment compared to the simply supported beam (SSB) case. The bending moment diagram of the EFM has a parabolic piece-wise shape with drops in the center of each panel equal to the product of the external rotational spring stiffness $k_{rot,f-w}$ and the rotation of each panel θ_i (see Figure 4).

To understand the effect of the external rotational springs on the bending moment diagram, a floor width B of 14m was analysed, with the same mechanical and geometrical properties used in previous analyses. The bending moment diagrams of the EFM and SSB, normalized with respect to the maximum value of the simply supported scheme, are reported in Figure 14. Note that the maximum normalized bending moment value ranges between 0.27 and 0.88. The latter value occurs in High-Low condition, where the EFM's bending moment distribution is similar to that of the SSB scheme. This occurs since in High-Low condition there is small rotation of the panels, because of high $K_{f-f,T}$, and low $k_{rot,f-w}$, due to low values of K_{f-w}. On the contrary, where the ratio between K_{f-w} and $K_{f-f,L}$ is equal or greater than one, the maximum normalized bending moments is equal to 0.27 or 0.28 and this highlights the contribution of the external rotational springs. Finally it can be noticed that for values of $K_{f-f,L}$, $K_{f-f,T}$ and K_{f-w} up to 10 N/mm^2, i.e. in more common situations in practical construction the maximum normalised bending moment ranges between 0.27 and 0.58. This shows the effect of the wall-to-floor connections.

5. Conclusion

The contributions described in Section 1.1 have been presented in this paper as follows:

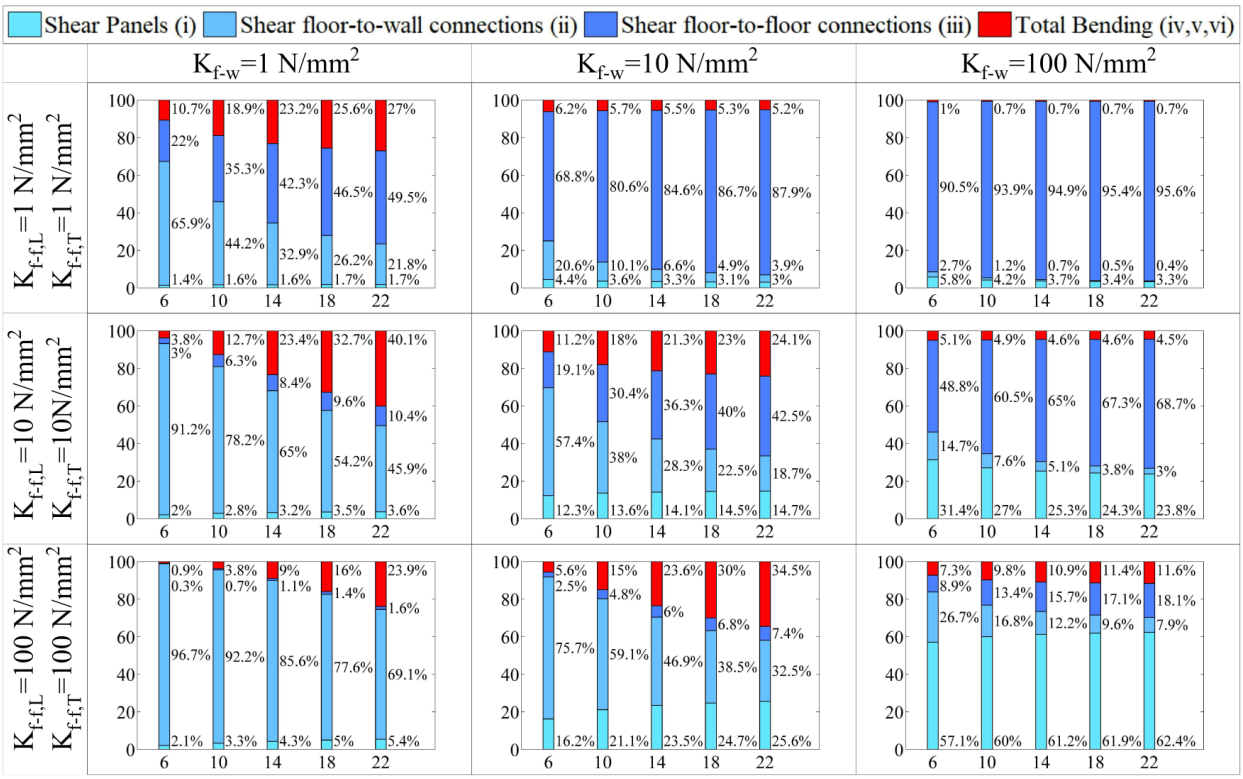

Fig. 11. Shear and global bending deformation contributions [%] against floor width $B[m]$, Case A ($K_{ff,L} = K_{ff,T}$).

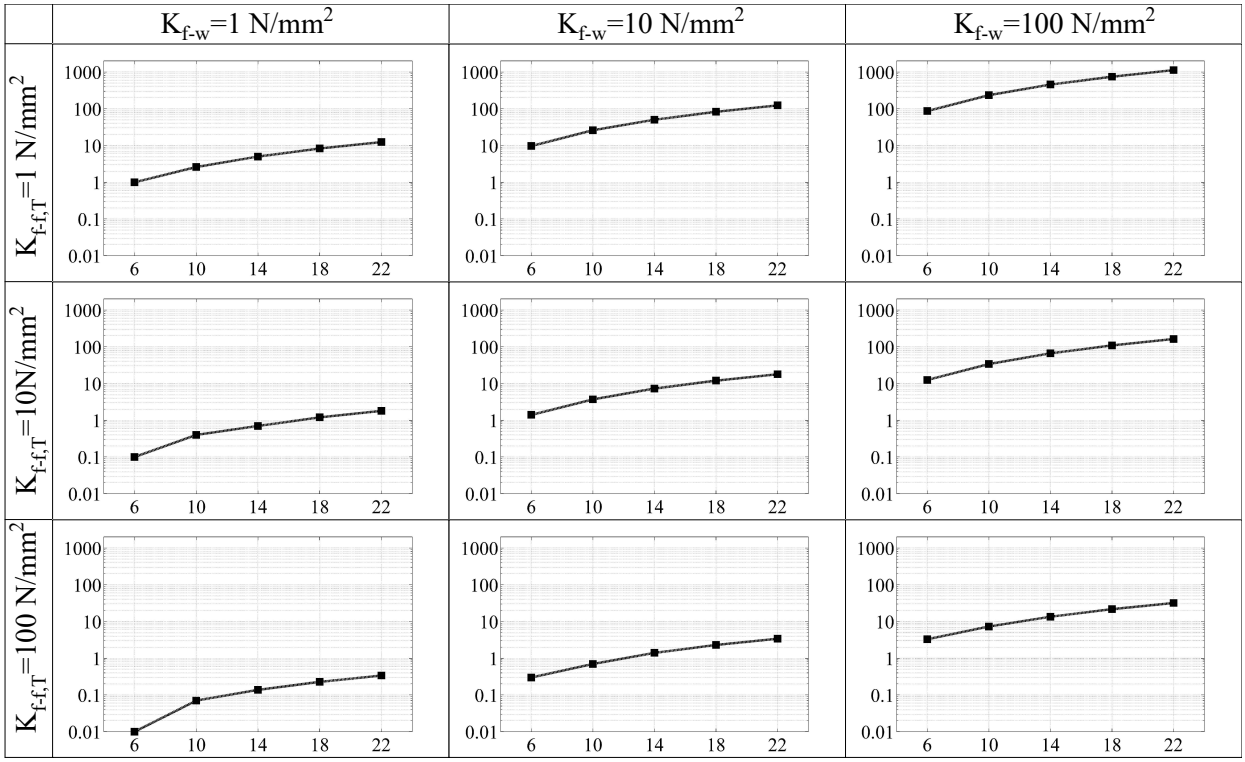

Fig. 12. The relative contribution of the floor-to-floor and floor-to-wall contributions in bending $\tilde{k}_B[-]$ (Eq. 10) against floor width B [m].

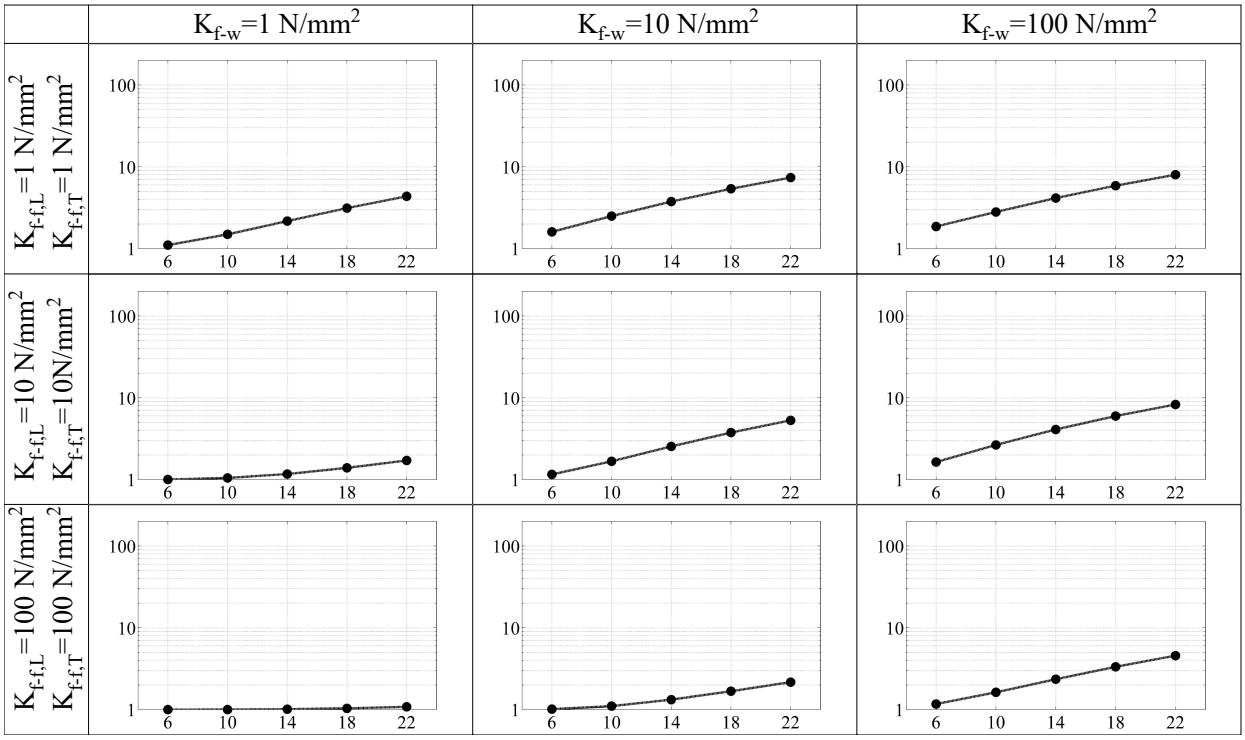

Fig. 13. Ratio between the maximum displacements without and with external rotational springs $\frac{\Delta^*}{\Delta}[-]$ against floor width $B[m]$, Case A ($K_{ff,L} = K_{ff,T}$).

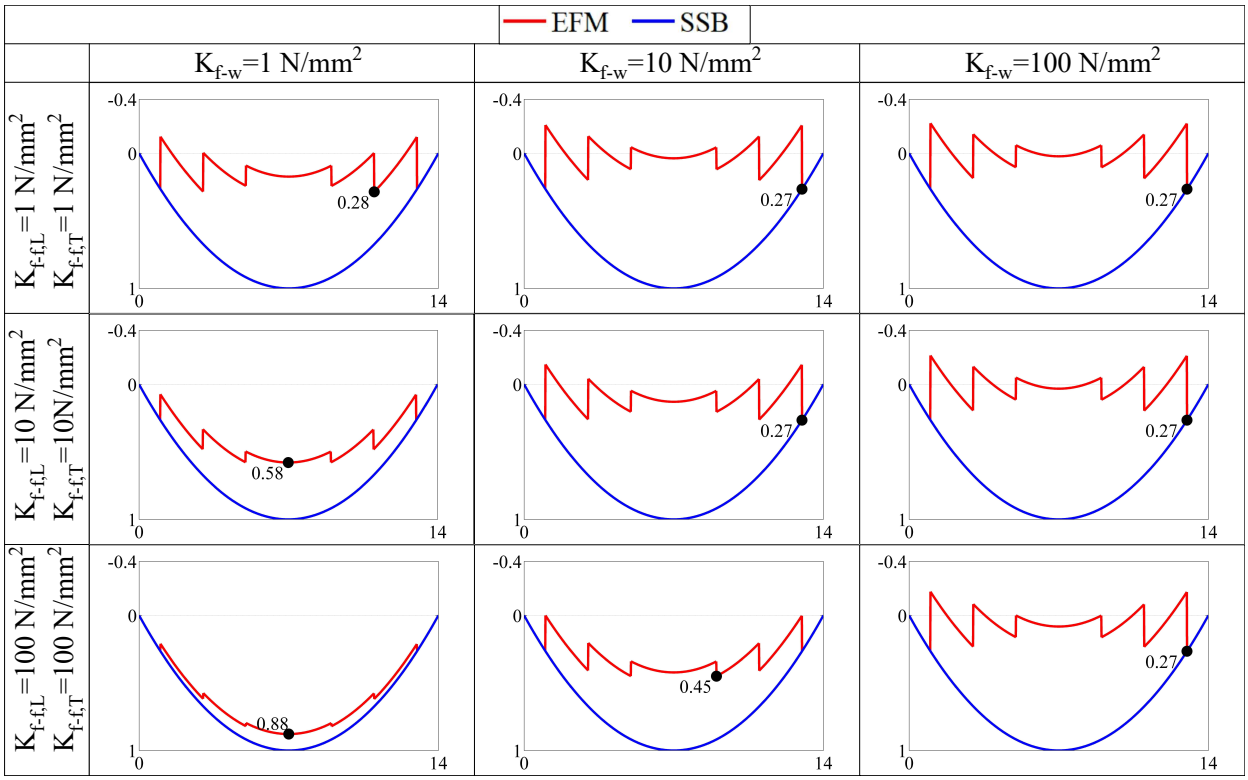

Fig. 14. Normalized bending moment diagrams of EFM and SSB, Case A ($K_{ff,L} = K_{ff,T}$).

1. A simplified equivalent frame model was developed to represent the in-plane flexibility of a CLT floor diaphragm, and validated using a planar finite element model. This study takes advantage of the low computational cost of the equivalent frame model to conduct an extensive sensitivity analysis to identify the most important deformation mechanisms which contribute to in-plane deformation in CLT floor diaphragms.

2. This study included the effect of the connection to the supporting walls below, which has not been considered in previous studies, and showed a substantial effect on the flexibility of the floor. It was shown that connection to the supporting walls redistributes the bending moment, but does not significantly affect the shear deformations between panels. The equivalent frame model captures this effect, where a simply supported beam model would not.

3. Under realistic connection stiffness, material properties and geometry, the stiffness of the diaphragm was not found to be sensitive to the thickness of the floor plate. The floor geometry and connection stiffness were the key influencing parameters. For this study, in which the aspect ratio of the floors is between 1.2 and 4.4, the flexibility of the floor diaphragm is generally dominated by slip between panels, rather than panel rotation or global in-plane bending. The flexibility is thus dependent on the stiffness of the connections under this type of load.

Acknowledgements

Tiziano Sartori (Rewis) is acknowledged for his fundamental support for the validation of numerical modellings and numerical analyses. Special thanks to Prof. M. Piazza for his precious suggestions. Thanks to Prof. Richard Harris, Dr. Wen-Shao Chang and Dr. Julie Bregulla for discussions in planning the experimental work. The experimental work was funded by a BRE Trust grant.

Appendix A: Sensitivity analysys - Case B

This section reports the results of sensitivity analysis for Case B. In this case the stiffness in the longitudinal direction varies from 1 to 100N/mm^2 while the the stiffness in the transversal direction is set to 1N/mm^2.

Similarly to Section 4.2, first the in-plane flexibility $\tilde{\Delta}$ is analysed by varying the thickness t and the width of the floor B. The results of thickness analysis are shown in Figure 15.

The same considerations made for Case A can be extended to the Case B. The greatest differences of in-plane flexibility between Case A and Case B occur for High-Low conditions. This occurs because when K_{f-w} is low the contribution of $K_{f-f,T}$ becomes more important. Consequently, substantial differences in the in-plane flexibility are observed in the last row of the matrices. On the other hand, when the K_{f-w} is high, the contribution of $K_{f-f,T}$ is negligible; so the High-High conditions are similar for Cases A and B.

The analysis of displacement due to shear and bending deformations for Case B is shown in Figure 16. It shows similar results to Case A. Shear is the major contribution for almost all cases. The only exception is the High-Low condition for Case B, with B equal to 22m. Here the shear contribution is 47.1%. Overall, the shear contribution ranges between 47.1 % and 99.3 %.

The greatest difference between Cases A and B is in the High-Low condition, where, for B equal to 22m, the bending contribution is 23.9% in Case A, and 52.9% in Case B. High values of bending contribution are reached for High-Low in Case B since, in this case, both external ($k_{rot,f-w}$) and internal ($k_{rot,f-f}$) rotational springs have minimum values, while the springs related to shear displacement ($k_{s,f-w}$ and $k_{s,f-f}$) are maximum.

The analysis on the effects of external rotational springs was performed also for the Case B. Figure 17 shows the results of the analysis on the displacements. It shows more marked results than Case A. In fact in this case, the ratio $\frac{\Delta^*}{\Delta}$ varies greatly, ranging between 1 and 133. The maximum value is reached in the High-High condition for Case B, for a floor width of 22 m. This is because Δ is lowest in High-High conditions (see Figures 10 and 15) and Δ^* is highest in Case B. The minimum occurs in the High-Low condition, with a floor width of 6m.

The greatest differences between Cases A and B are in the High-High condition. Furthermore, the values of $\frac{\Delta^*}{\Delta}$ in Case B are greater than those in Case A for all stiffness conditions.

Finally the effect of distribution of the bending moment was analysed and the results are depicted in Figure 18. Also in this case more marked results than Case A have been found. The bending moment distribution is almost equal in all conditions and it is very close to condition of infinitely rigid external rotational spring ($k_{rot,f-w} \rightarrow \infty$). In High-Low condition the bending moment law of the EFM has lower values than those of the Case A, since the rotations of the panels reach higher values due to the lower values of the $K_{f-f,T}$. This is also

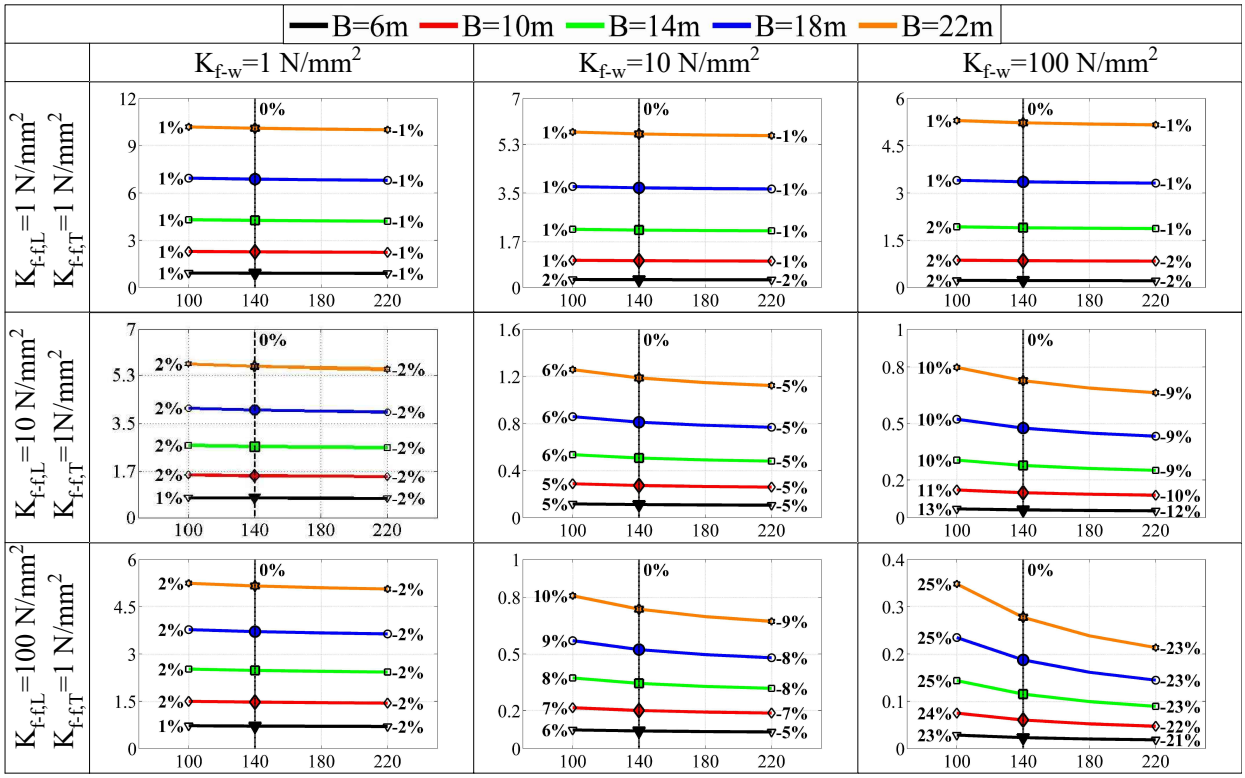

Fig. 15. In-plane flexibility $\tilde{\Delta}[\frac{mm^2}{N}]$ plotted against panel thickness $t[mm]$, Case B ($K_{ff,T} = 1N/mm^2$).

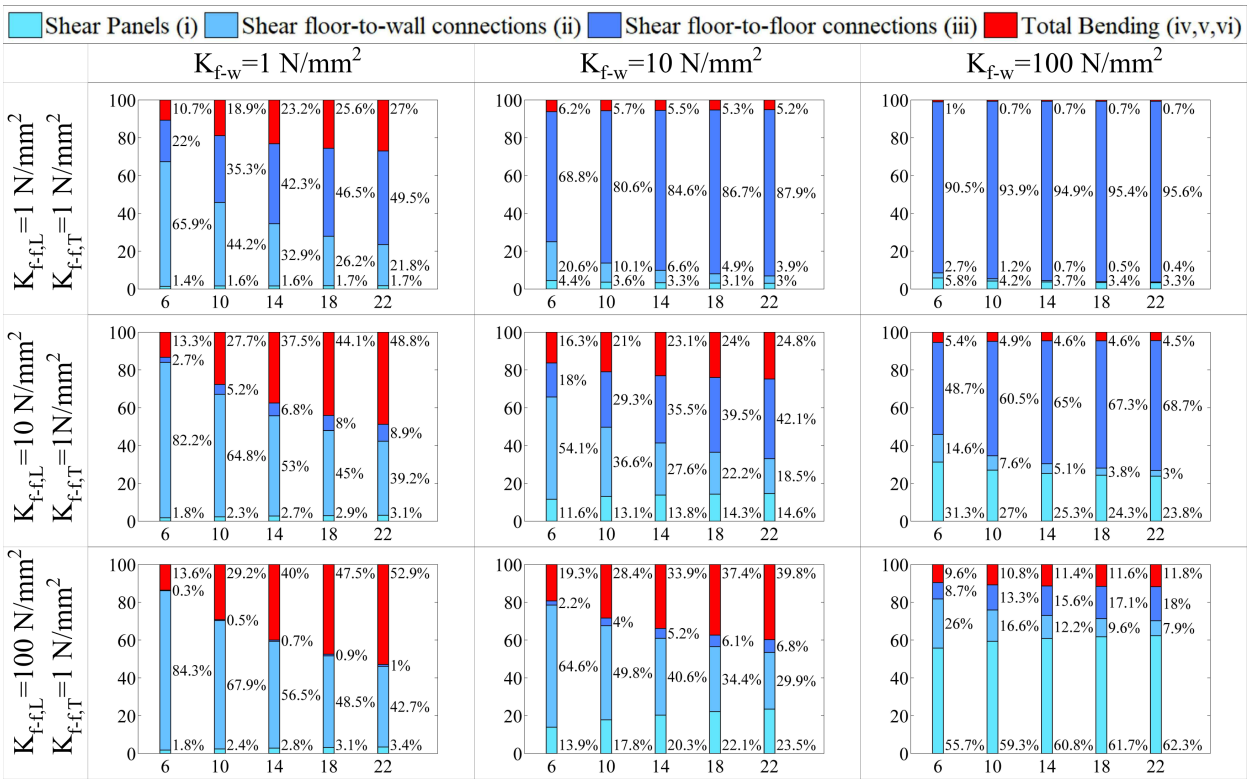

Fig. 16. Shear and global bending deformation contributions [%] against floor width $B[m]$, Case B ($K_{ff,T} = 1\ N/mm^2$).

the condition where Cases A and B have the greater differences.

Appendix B: Case Study

In this section a case study is presented: the mechanical parameters studied in previous sections are evaluated using the EFM. Consider a floor with a width B equal to 10m and a length L equal to 5m; a horizontal uniformly distributed load q of 2.5kN/m is applied. The floor is made with 5-layered panels of thickness t and width b equal to 160mm (40L-20T-40L-20T-40L) and 2m respectively. Screwed wall-to-floor and floor-to-floor connection were chosen for this case study. The floor-to-floor connection was formed by a "spline-joint", *i.e.* a wooden board which connects mutually two contiguous panels by screws. Screws 8×240mm and 8×140mm were chosen for the wall-to-floor and floor-to-floor connections respectively. For both connections a spacing s of 300mm was considered.

The stiffness k_{ser} of the wall-to-floor and floor-to-floor connections, evaluated according to Eurocode 5 [24], is equal to 3.32kN/mm and 1.66kN/mm respectively.

The stiffness per unit of length of both wall-to-floor and floor-to-floor connections can be evaluated using Eq. (12) and Eq. (13)

$$K_{f-w} = \frac{k_{ser,f-w}}{s} = 11.07 N/mm^2 \tag{12}$$

$$K_{f-f,L} = K^{+}_{f-f,T} = \frac{k_{ser,f-f}}{s} = 5.53 N/mm^2 \tag{13}$$

The stiffness per unit of length $K^{-}_{f-f,T}$ was evaluated with Eq. (7) having considered a modulus of elasticity E_0 equal to 12000MPa.

The stiffness of the EFM springs can be evaluated using Eq. (3 to 6). The values of stiffness of these springs are reported in the Table (1). Using the latter stiffness values, the geometry and the load indicated above, the EFM provides the values indicated in Table (2).

It can be observed that the maximum displacement, equal to 0.78mm, is due mainly to the connections. Indeed the shear contribution from floor-to-floor *ii)* and wall-to-floor *iii)* connections account for almost the 75% of the total deformation. Only 10% is due to shear in

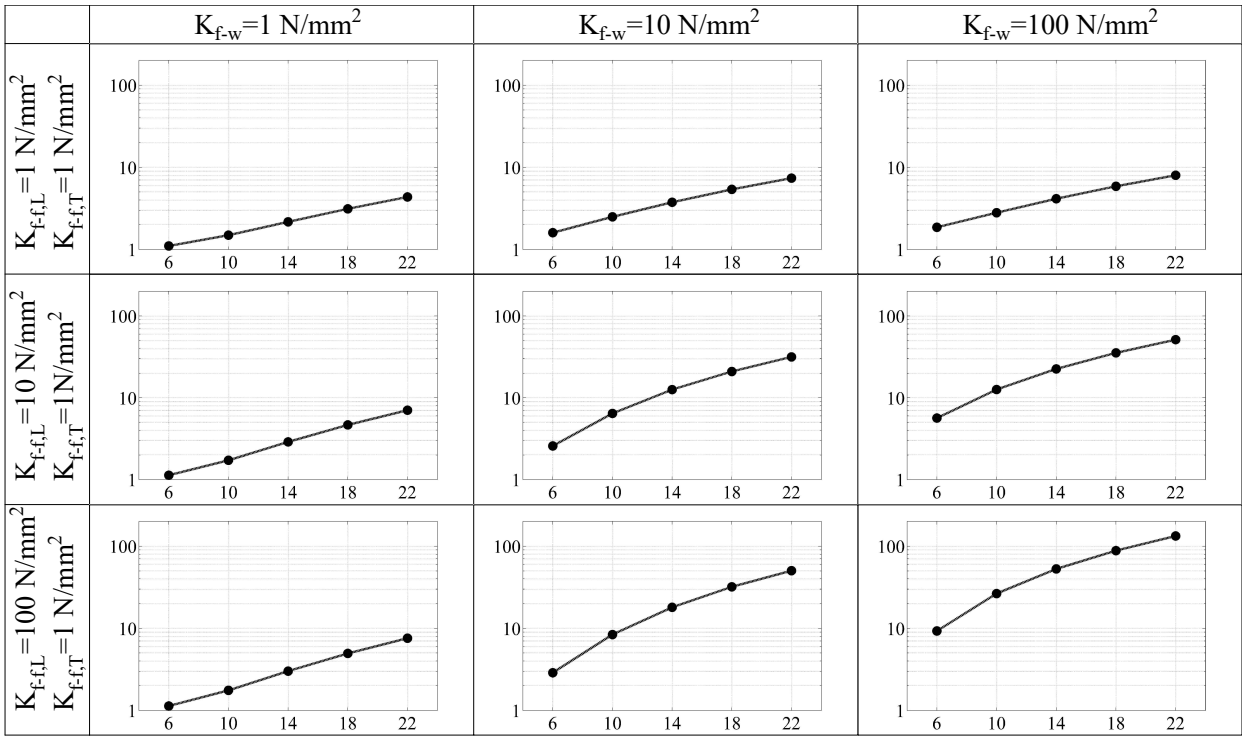

Fig. 17. Ratio between the maximum displacements without and with external rotational springs $\frac{\Delta^*}{\Delta}[-]$ against floor width $B[m]$, Case B ($K_{ff,T} = 1N/mm^2$).

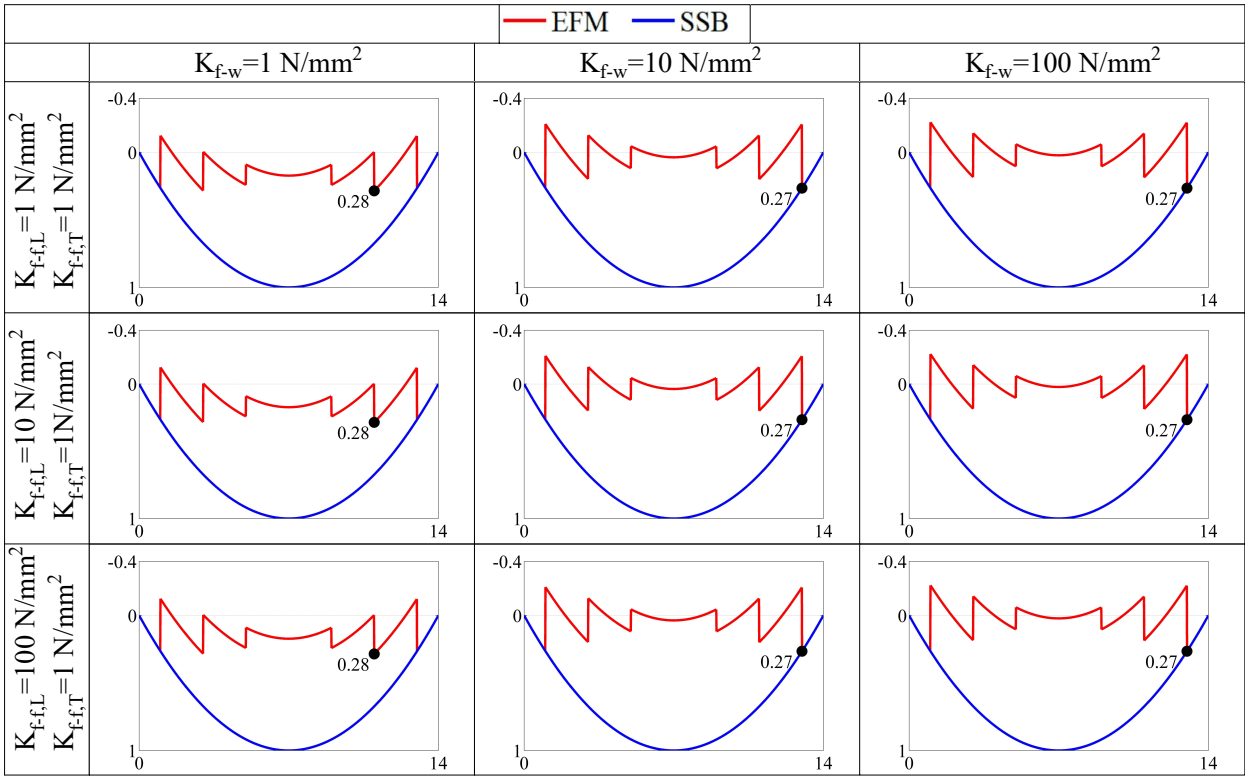

Fig. 18. Normalized bending moment diagrams of EFM and SSB, Case B ($K_{ff,T} = 1N/mm^2$).

$k_{s,f-w}$	$k_{s,f-f}$	$k_{rot,f-w}$	$k_{rots,f-f}$
[N/mm]	[N/mm]	[kNm]	[kNm]
55.350	27.650	453.900	178.000

Table 1. Springs stiffness values of the EFM

the panels *i)* whereas 15% is related to the total bending contribution *iv) v) vi)*. The ratio $\frac{k_{vi}}{k_{iv,v}}$ of 4.90 highlights the importance of the stiffening effect due to the external rotational springs $k_{rot,f-w}$, which derives from the wall-to-floor connections. This effect can be also noticed from the ratio $\frac{\Delta^*}{\Delta}$, showing a reduction of 74% of the maximum displacement for the stiffening effect of external rotational springs $k_{rot,f-w}$. Finally, an important reduction of the maximum bending moment compared to the simply supported scheme is observed.

References

[1] CEN, BS EN 1998-1:2004 Eurocode 8 : Design of structures for earthquake resistance - Part 1: General rules, seismic actions and rules for buildings, 2013.

[2] P. W. Somers, National Earthquake Hazards Reduction Program P-751. Chapter 11: Wood Design, 2009.

[3] J. P. Moehle, J. D. Hooper, D. J. Kelly, T. R. Meyer, Seismic Design of Cast-In-Place Concrete Diaphragms, Chords, and Collectors, 2010.

[4] D. Ahmed, A. Asiz, Structural performance of hybrid multistorey buildings with massive timber-based floor elements loaded under extreme lateral loads, International Journal of Computational Methods and Experimental Measurements 5 (2017) 905–916. doi:10.2495/CMEM-V5-N6-905-916.

[5] S. Ashtari, T. Haukaas, F. Lam, In-Plane Stiffness of Cross-Laminated Timber Floors, in: World Conference on Timber Engineering, 2014.

[6] Z. Chen, Y.-H. Chui, G. Doudak, C. Ni, M. Mohammad, Simulation of the Lateral Drift of Multi-Storey Light Wood Frame Buildings Based on a Modified Macro-Element Model, in: World Conference on Timber Engineering, Quebec City, Canada, 2014.

[7] Z. Chen, Y. H. Chui, C. Ni, G. Doudak, M. Mohammad, Load Distribution in Timber Structures Consisting of Multiple Lateral Load Resisting Elements with Different Stiffnesses, Journal of Performance of Constructed Facilities 28 (2014) A4014011. doi:10.1061/(ASCE)CF.1943-5509.0000587.

[8] D. Moroder, F. Sarti, S. Pampanin, Higher mode effects in multi-storey timber buildings with varying diaphragm flexibility, in: New Zealand Society for Earthquake Engineering (NZSEE) Annual Technical Conference, Christchurch, 2016.

[9] A. Filiatrault, D. Fischer, B. Folz, C.-M. Uang, Experimental parametric study on the in-plane stiffness of wood diaphragms, Canadian Journal of Civil Engineering 29 (2002) 554–566. doi:10.1139/l02-036.

[10] S. Pei, J. V. D. Lindt, M. Popovski, Approximate R-Factor for Cross Laminated Timber Walls in Multi-Story Buildings, Journal of Architectural Engineering 19 (2012) 245–255. doi:10.1061/(ASCE)AE.1943-5568.0000117.

[11] S. Pei, M. Popovski, J. W. Van de Lindt, Analytical study on seismic force modification factors for cross-laminated timber buildings, Canadian Jornal of Civil Engineering 40 (2013) 887–896. doi:10.1139/cjce-2013-0021.

[12] I. Gavric, M. Fragiacomo, A. Ceccotti, Cyclic behavior of typical screwed connections for cross-laminated (CLT) structures, European Journal of Wood and Wood Products 73 (2015) 179–191. doi:10.1007/s00107-014-0877-6.

[13] Z. Li, M. He, Z. Ma, K. Wang, R. Ma, In-Plane Behavior of Timber-Steel Hybrid Floor Diaphragms: Experimental Testing and Numerical Simulation, Journal of Structural Engineering 142 (2016) 04016119. doi:10.1061/(ASCE)ST.1943-541X.0001601.

[14] C. Loss, M. Piazza, R. Zandonini, Connections for steel–timber hybrid prefabricated buildings. Part I: Experimental tests, Construction and Building Materials 122 (2016) 781–795. doi:10.1016/j.conbuildmat.2015.12.002.

[15] A. Hossain, M. Popovski, T. Tannert, Cross-laminated timber connections assembled with a combination of screws in withdrawal and screws in shear, Engineering Structures 168 (2018) 1–11. doi:10.1016/j.engstruct.2018.04.052.

[16] K. Sullivan, T. H. Miller, R. Gupta, Behavior of cross-laminated timber diaphragm connections with self-tapping screws, Engineering Structures 168 (2018) 505–524. doi:10.1016/j.engstruct.2018.04.094.

[17] C. Loss, A. Frangi, Experimental investigation on in-plane stiffness and strength of innovative steel-timber hybrid floor diaphragms, Engineering Structures 138 (2017) 229–244. doi:10.1016/j.engstruct.2017.02.032.

[18] C. Loss, S. Rossi, T. Tannert, In-plane stiffness of hybrid steel-cross-laminated timber floor diaphragms, Journal of Structural Engineering (United States) 144 (2018). doi:10.1061/(ASCE)ST.1943-541X.0002105.

[19] D. Moroder, T. Smith, S. Pampanin, A. Palermo, A. H. Buchanan, Design of floor diaphragms in multi-storey timber buildings, in: New Zealand Society for Earthquake Engineering (NZSEE) Annual Technical Conference, Rotorua, 2015.

[20] D. Moroder, S. Pampanin, A. Buchanan, Floor Diaphragms in Timber Buildings, Forest and Wood Products Australia, Melbourne, Australia, 2016.

[21] A. Ceccotti, C. Sandhaas, M. Okabe, M. Yasumura, C. Minowa, N. Kawai, SOFIE project – 3D shaking table test on a seven-storey full-scale cross-laminated timber building, Earthquake Engineering & Structural Dynamics 42 (2013) 2003–2021.

[22] M. Yasumura, K. Kobayashi, M. Okabe, T. Miyake, K. Matsumoto, Full-Scale Tests and Numerical Analysis of Low-Rise CLT Structures under Lateral Loading, Journal of Structural Engineering 142 (2016) E4015007. doi:10.1061/(ASCE)ST.1943-541X.0001348.

[23] M. Popovski, I. Gavric, Performance of a 2-Story CLT House Subjected to Lateral Loads, Journal of Structural Engineering 142 (2016) E4015006. doi:10.1061/(ASCE)ST.1943-541X.0001315.

[24] CEN, BS EN 1995 Eurocode 5: Design of timber structures - Part 1-1: General - Common rules and rules for buildings, 2014.

[25] M. Dorn, K. de Borst, J. Eberhardsteiner, Experiments on dowel-type timber connections, Engineering structures (Online) 47 (2013) 67–80.

[26] T. Reynolds, R. Harris, W.-S. Chang, Viscoelastic embedment behaviour of dowels and screws in timber under in-service vibration, European Journal of Wood and Wood Products 71 (2013) 623–634. doi:10.1007/s00107-013-0720-5.

[27] M. Izzi, D. Casagrande, S. Bezzi, D. Pasca, M. Follesa, R. Tomasi, Seismic behaviour of cross-laminated timber structures: A state-of-the-art review, Engineering Structures 170 (2018) 42–52. doi:10.1016/j.engstruct.2018.05.060.

[28] H. Blass, P. Fellmoser, Design of solid wood panels with cross

Δ	*i)*	*ii)*	*iii)*	*iv) v) vi)*	$\frac{k_{vi}}{k_{iv,v}}$	$\frac{\Delta^*}{\Delta}$	$\frac{M_{max}^{EFM}}{ql^2/8}$
[mm]	[%]	[%]	[%]	[%]	[-]	[-]	[-]
0.78	10.0	28.8	46.1	15.1	4.90	1.74	0.36

Table 2. Values of mechanical parameters according to sensitivity analyses of Sections 4.2 and 4.3

layers, World Conference on Timber Engineering WCTE, Lathi, Finland (2004).

[29] R. Brandner, P. Dietsch, J. Dröscher, M. Schulte-Wrede, H. Kreuzinger, M. Sieder, Cross laminated timber (CLT) diaphragms under shear: Test configuration, properties and design, Construction and Building Materials 147 (2017) 312 – 327. doi:https://doi.org/10.1016/j.conbuildmat.2017.04.153.

[30] CEN, EN 1995-1-1:2004/A2:2014 - Design of Timber structures. Part 1-1: General - Common rules and rules for buildings La , 2004.

[31] D. Casagrande, S. Rossi, T. Sartori, R. Tomasi, Proposal of an analytical procedure and a simplified numerical model for elastic response of single-storey timber shear-walls, Construction and Building Materials 102 (2016) 1101–1112. doi:10.1016/j.conbuildmat.2014.12.114.

[32] G. Tamagnone, G. Rinaldin, M. Fragiacomo, A novel method for non-linear design of clt wall systems, Engineering Structures 167 (2018) 760–771. doi:10.1016/j.engstruct.2017.09.010.

[33] CEN, BS EN 12512:2001 Timber structures. Test methods. Cyclic testing of joints made with mechanical fasteners, 2001.